



- 1 A new biogeochemical modelling framework (FLaMe v1.0) for lake methane
- 2 emissions on the regional scale: Development and application to the European
- 3 domain
- 4 Manon Maisonnier¹, Maoyuan Feng^{1*}, David Bastviken², Sandra Arndt¹, Ronny Lauerwald³, Aidin
- 5 Jabbari⁴, Goulven Gildas Laruelle¹, Murray D. MacKay⁵, Zeli Tan⁶, Wim Thiery⁷, Pierre Regnier¹
- 6 ¹Biogeochemistry and Modelling of the Earth System-BGEOSYS, Department of Geoscience,
- 7 Environment and Society, Université Libre de Bruxelles, Brussels, Belgium
- 8 ²Linköping University, Department of Thematic Studies, Tema Environmental Change, Sweden
- 9 ³ Université Paris-Saclay, INRAE, AgroParisTech, UMR Ecosys, Palaiseau, France
- ⁴Environmental Fluid Dynamics Laboratory, Department of Civil Engineering, Queen's University,
- 11 Kingston, ON, Canada
- 12 ⁵Science and Technology Branch, Environment and Climate Change Canada, Toronto, M3H5T4,
- 13 Canada

- 14 ⁶Pacific Northwest National Laboratory, Richland, WA, USA
- 15 ⁷Department of Water and Climate, Vrije Universiteit Brussel, Brussels, Belgium

*Correspondence to Maoyuan Feng (maoyuan.feng@ulb.be)





Abstract

18

19 This study presents a new physical-biogeochemical modelling framework for simulating lake 20 methane (CH₄) emissions at regional scales. The new model, FLaMe v1.0 (Fluxes of Lake Methane), 21 rests on an innovative, computationally efficient lake clustering approach that enables the simulation 22 of CH₄ emissions across a large number of lakes. Building on the Canadian Small Lake Model (CSLM) 23 that simulates the lake physics, we develop a suite of biogeochemical modules to simulate transient 24 dynamics of organic Carbon (C), Oxygen (O2), and CH4 cycling. We first test the performance of 25 FLaMe by analyzing physical and biogeochemical processes in two representative lakes (an 26 oligotrophic, deep lake driven by cold climate versus a trophic, shallow lake driven by warm climate). 27 Next, we evaluate the model by comparing simulated and observed timeseries of CH₄ emissions in 28 four well-surveyed lakes. We then apply FLaMe at the European scale to evaluate simulated diffusive 29 and ebullitive lake CH₄ fluxes against in-situ measurements in both boreal and central European 30 regions. Finally, we provide a first assessment of the spatio-temporal variability in CH₄ emissions 31 from European lakes smaller than 1000 km² (n=108407, total area = 1.33x10⁵ km²), indicating a total 32 emission of 0.97±0.23 Tg CH₄ yr⁻¹, with the uncertainty constrained by combining FLaMe and 33 machine learning techniques. Moreover, 30% and 70% of these CH₄ emissions are through diffusive 34 and ebullitive pathways, respectively. Annually averaged CH₄ emission rates per unit lake area during 35 2010–2016 have a South-to-North decreasing gradient, resulting in a mean over the European domain as 7.39 g CH₄ m⁻² yr⁻¹. Our simulations reveal a strong seasonality in European lake CH₄ emissions, 36 37 with late summer emissions nearly ten times higher than winter values. This pronounced seasonal 38 variation highlights the importance of accounting for the sub-annual variability in CH₄ emissions to 39 accurately constrain regional CH₄ budgets. In the future, FLaMe could be embedded into Earth 40 System Models to investigate the feedback between climate warming and global lake CH₄ emissions.





1. Introduction

42 Methane (CH₄) is the second most important greenhouse gas after carbon dioxide (CO₂), with a 43 Global Warming Potential (GWP) per mass ~28 times higher than that of CO₂ over a 100-year horizon 44 (Saunois et al., 2020). Over the last centuries, the atmospheric CH₄ concentration has increased from 45 722 ppb in the pre-industrial period (year 1750) to 1923 ppb in year 2023 (Saunois, et al., 2020; 46 Dlugokencky, 2022; Forster et al., 2024) and this increase is expected to continue in the future. The 47 critical role of CH₄ in global warming has called for the establishment of a comprehensive global 48 CH₄ budget, which embraces both natural and anthropogenic sources (Saunois et al., 2016; 2020; 49 2024). This budget identified inland waters (wetlands, lakes, reservoirs, ponds, rivers, etc.) as an 50 important, yet highly uncertain atmospheric CH₄ source (Jackson et al., 2020, 2024; Saunois, et al., 51 2020, Canadell et al., 2021). Global lake CH₄ emissions, which has been estimated to account for ~5 52 to 20% of total CH₄ emissions (576 TgCH₄ yr⁻¹), are the largest contributors to this inland water 53 source (Jackson et al., 2020; Saunois et al., 2020). However, estimates of its magnitude vary 54 depending on the assessment methods, with discrepancies of up to a factor of four (Saunois et al., 55 2020; DelSontro and John 2018; Rosentreter et al., 2021; Bastviken et al., 2011; Deemer et al., 2016; 56 Johnson et al., 2021; Holgerson and Raymond 2016; Stavert et al. 2022). This variability in global 57 estimates also manifests itself at the continental scale. For instance, estimates of European lake 58 methane emissions range from 0.9 to 2.5 Tg CH₄ yr⁻¹ (Petrescu et al. 2021, 2023; Lauerwald et al., 59 2023). 60 Observation-based upscaling approaches are highly dependent on the availability and quality of 61 in-situ measurements, which are unevenly distributed across the globe and biased towards summer 62 months (Canadell et al., 2021; Johnson et al., 2022). Although the number of CH4 emission





databases together contain only 1081 records from 575 lakes worldwide (Rosentreter et al., 2021; 64 65 Johnson et al., 2022). This relatively small data compilation is unlikely to capture the full diversity 66 of physical and biogeochemical patterns of >1.4 million lakes worldwide, which vary by morphology, 67 climate, trophic status, and underlying sediment characteristics (Rinta et al., 2017; Bastviken 2004, 68 2022; Deemer and Holgerson 2021; Johnson et al., 2022). Even more critically, the underlying data 69 collection was not designed to capture the inter-annual and decadal variability in CH₄ emissions 70 driven by climate change and nutrient dynamics, hence rendering the decomposition of the total lake 71 CH₄ fluxes into natural and human-induced components challenging (Saunois et al., 2020). Finally, 72 although current instruments and techniques can effectively capture CH₄ fluxes through diffusive 73 (driven by gradients of aqueous CH₄ concentrations) and ebullitive (via gas bubbles in the sediments due to oversaturation) emission pathways, measurements related to lake turnover events (release of 74 75 previously accumulated CH₄ due to stratification and ice cover) remain highly challenging (Denfeld 76 et al., 2018; Mayr et al., 2020; Zimmermann et al., 2019). These limitations induce large uncertainties 77 in observation-based upscaling methods. In this context, process-based modelling approaches - that 78 rely on detailed representations of lake physical and biogeochemical processes informed and tested 79 with the available observational data - offer complementary strategies to help reduce these 80 uncertainties. 81 Process-based biogeochemical models provide powerful tools to upscale scarce observations, 82 both in space and in time. In combination with the available observational datasets, they can help 83 deliver regional and global estimates of lake CH₄ emissions from daily to decadal timescales, as well 84 as future projections. These mechanistic models can also help identify the drivers such as climate, 4

measurements from lakes has increased considerably in recent decades, the two largest current

https://doi.org/10.5194/egusphere-2025-1306 Preprint. Discussion started: 28 March 2025 © Author(s) 2025. CC BY 4.0 License.



85

86

87

88

89

90

91

92

93

94

95

96

97

98

99

100

101

102

103

104

105

106



land-use and atmospheric composition changes responsible for the complex temporal dynamics of lake CH₄ emissions. Over the last decades, several process-based models have thus emerged, e.g., LAKE 2.0 (Stepanenko et al. 2016), bLake4Me (Tan et al., 2015), and ALBM (Tan et al., 2018; 2024), to estimate lake CH₄ emissions to the atmosphere. These models explicitly account for the physical and biogeochemical processes that govern lake CH₄ dynamics and resulting emissions. For instance, using ALBM, Zhuang et al. (2023) recently estimated that global lakes (larger than 0.1 km²) emit 24.0 ± 8.4 Tg CH₄ yr⁻¹, which is at the lower end of the range reported by Saunois *et al.* (2020) and represents 11% of total global CH₄ emissions from natural sources as estimated from atmospheric inversions. Yet, these process-based models also have limitations that need to be addressed. A central limitation is the omission of lake phytoplankton productivity, which is one of the most reactive organic C sources and thus substrates for CH₄ production. In most of existing models, this key process and the associated microbial degradation of organic C is not simulated explicitly but taken as prescribed model inputs. If phytoplankton productivity and associated contributions of methane substrates can be incorporated in lake CH₄ models, this would allow capturing the impacts of environmental conditions beyond the commonly included direct temperature effects on organic matter decomposition and CH₄ production. Such additional important impacts include feedback of C metabolism on lake oxygen (O2) cycling along with eutrophication effects on CH4 emissions (Del Sontro et al., 2018; Rosentreter et al., 2021; Stavert et al., 2022). However, including an explicit description of these processes is challenging, because it requires to account for a suite of key physical and biogeochemical processes controlling the coupled C-O₂-CH₄ cycles while at the same time maintaining model complexity, as well as the needs for observational data and computational costs for regional and global scale applications with tractable bounds. In addition, it also requires the





quantification of nutrient inputs from the surrounding catchments, which exert a key control on lake productivity.

To tackle with these challenges, we here develop a new process-based model framework of intermediate complexity, FLaMe v1.0 (Fluxes of Lake Methane version 1.0, hereafter referred as FLaMe) that couples the C-O₂-CH₄ cycles in lakes using a one-dimensional representation. Specifically, FLaMe builds upon the existing physical lake model CSLM (Canadian Small Lake Model–MacKay, 2012; MacKay *et al.*, 2017), and extends with a novel biogeochemical module that captures the production, oxidation, storage, transport and emissions of CH₄ in/from lakes. Importantly, FLaMe introduces lake primary production and turnover of autochthonous organic carbon as a major driver of lake O₂ and CH₄ dynamics. The coupled, mechanistic lake model is then embedded in a computationally efficient clustering approach that allows for the application of the new, coupled, mechanistic lake model for (i) large parameter/input ensemble runs on regional/global scales for uncertainty assessments, (ii) long-term model projections for the assessment of future climate change and its feedback on the Earth system, (iii) a potential coupling to ESMs in subsequent stages of its development.

The structure of this paper is described as follows. In section 2, we provide a general description of the lake model with a focus on a detailed description of the novel biogeochemical modules, as well as the parameter choices and numerical solutions. In section 3, we first test the overall behavior of FLaMe using two representative lakes (an oligotrophic, deep lake driven by cold climate *versus* a trophic, shallow lake driven by warm climate), and then evaluate the simulated temporal variations of CH₄ fluxes against observational data at four well-surveyed lakes in real world. Next, we apply

https://doi.org/10.5194/egusphere-2025-1306 Preprint. Discussion started: 28 March 2025 © Author(s) 2025. CC BY 4.0 License.





FLaMe at the European scale and evaluate the results against *in-situ* measurements in boreal and central European lakes compiled by Rinta *et al.* (2017). Finally, we provide a spatio-temporally resolved estimate of CH₄ emissions from European lakes (2010–2016), assess their sensitivity to key model parameters, and constrain their uncertainty range using a machine-learning approach. In section 4, we discuss model limitations and potential directions for further research. Main conclusions and outlooks are drawn in section 5.

2. Methodology

2.1 General model approach

We developed a new process-based physical-biogeochemical model, FLaMe v1.0 (Fluxes of Lake Methane), to simulate lake CH₄ production and emission at large spatial scales. FLaMe resolves the interplay of physical and biogeochemical processes that governs organic matter ($C_{OC,auto}$), oxygen (O_2), and methane (CH₄) dynamics to estimate (diffusive and ebullitive) lake CH₄ emissions, as well as CH₄ storage fluxes due to lake turnover and ice melting. To enable a continental-scale application of FLaMe (e.g., in Europe, n=108407 and total area = 1.33×10^5 km² for lakes with $0.1 \le A_0 \le 1000$ km² according to Messager *et al.*, 2016; A_0 is the lake surface area), we here propose a lake clustering strategy to reduce the computational and data/input costs (Fig. 1) while resolving the variability in lake sizes, morphology, and trophic status as well as climate conditions across Europe. Within each grid cell ($2.5^{\circ} \times 2.5^{\circ}$), lakes are binned into four classes according to surface area (0.1-1 km², 1-10 km², 10-100 km², 100-1000km²). We then run a FLaMe set-up for one representative lake per size class within each grid cell, using the arithmetic means of lake area, depth and trophic status of all lakes pertaining to the respective size class across the respective grid cell. The total emission flux





- from a given size class can be obtained by multiplying the CH₄ emission rates simulated by FLaMe with the total lake area of this size class (Fig. 1).
 - Meteorology Gridding & Clustering (1)

 Clustering Clustering Physical model

 Thermo

 Biogeochemical model

 Characteristics Upscaling (3)

Fig. 1. Illustration of the lake clustering and upscaling strategy for the continental application of FLaMe (Europe as an example). (1) Gridding and clustering: The European domain was divided into grid cells at a coarse spatial resolution of 2.5°×2.5°. Within each grid cell, lakes are clustered into four classes according to their surface areas. (2) FLaMe parallelization: FLaMe simulates the lake metabolic dynamics, vertically resolved concentration and rate profiles of the coupled O₂-CH₄ cycle as well as diffusive and ebullitive CH₄ fluxes through the water-air interface. The model was parallelized under transient conditions for each grid cell and each lake class. (3) Upscaling: The areal rates (i.e., fluxes per unit lake surface area) simulated by FLaMe were then multiplied by the total surface area of each lake class within each grid cell (available from HydroLAKES) and aggregated at the monthly timescale. The arrows pertaining to clustered and original lakes represent the CH₄ emissions.

2.2 Model description

FLaMe builds on an online coupling approach between the Canadian Small Lake Model (CSLM; MacKay, 2012; MacKay *et al.*, 2017) – a widely used lake physics model (Garnaud *et al.*, 2022; Verseghy and MacKay, 2017; William *et al.*, 2014) – and a set of newly developed biogeochemical





modules that resolve lake OC, O_2 and CH_4 dynamics. CSLM simulates the physical variables of temperature profile (T), thermocline depth (h_{mix}), photic depth (h_{phot}), and ice cover, which will be used to force the biogeochemical modules (Fig. 2). In turn, the biogeochemical module will later modify the photic depth simulated by CSLM to account for the effect of phytoplankton growth and self-shading on light penetration, thus resolving the feedback between lake biogeochemical processes and lake physical dynamics, hence forming a complete feedback loop. A detailed description of the well-established CSLM model can be found in MacKay (2012) and MacKay *et al.* (2017) and is also briefly presented in Supplementary Text S1. In what follows, we provide a detailed description of the vertically resolved 1D model set-up (section 2.2.1) used here, as well as of the novel biogeochemical modules (section 2.2.2 and Table 1 for selected model parameter values).

2.2.1 Model Scope: Idealized representation of lake morphology

Figure 2 illustrates the vertically resolved, one-dimensional model set-up of FLaMe that is used for both the physical and biogeochemical modules. The original version of CSLM usually adopts a "bucket" shaped morphology which assumes a constant area (A) versus water depth (z), i.e., $A(z) = A_0$, where A_0 is the lake surface area at z = 0 m. However, this morphology is unsuitable for the simulation of biogeochemical processes, especially when the variations in water depth within each lake are important. Therefore, we, instead, adopted a "valley" shaped lake morphology, with lake area A(z) given by:

183
$$A(z) = \frac{A_0}{2s} (s + \operatorname{arctanh}((1 - 2(z/h_{\max})) \tanh(s)))$$
 (1)

where A is the lake area (m²), z is the water depth (m), s is a shape parameter that controls the slope of the lakebed (a larger s indicates a steeper slope), and h_{max} is the maximum lake depth. To ensure

https://doi.org/10.5194/egusphere-2025-1306 Preprint. Discussion started: 28 March 2025 © Author(s) 2025. CC BY 4.0 License.





that the volume (and hence heat exchange) is conserved between the "bucket" and "valley" shape setups, the maximum depth of the valley-shape lake, h_{max} , must be twice that of the mean depth of the bucket-shape lake, h_{mean} (i.e., $h_{\text{max}} = 2h_{\text{mean}}$), which was extracted from the global HydroLAKES database compiled by Messager *et al.* (2016). The bottom temperature profiles simulated by CSLM were then extended to the maximal depth of the valley shape lake.

Physical processes in the water column are simulated by CSLM, on a one-dimensional, vertically resolved, evenly distributed grid with a grid spacing of 50 cm. Each water layer is connected to a vertically integrated lake sediment column of 5 m depth (h_s , m) (Fig. 2). Since the CH₄ production rate decreases exponentially with sediment depth, it is typically negligible at 5 m within the sediment column, thus ensuring that the total, depth-integrated benthic CH₄ production becomes insensitive to this arbitrary choice (Langenegger *et al.*, 2019). The surface area of each sediment column in contact with the water column is determined by difference in the widths of two adjacent water layers A(z) (Eq. (1)). In addition, it should be noted that we assume no *horizontal* material exchanges (O₂ and CH₄) between the sediments and water columns (i.e., across the interface where left and right edges of a water layer touch the sediment box; Fig. 2), while only the vertical exchanges are simulated in this first version of the model (see details in the following sections).





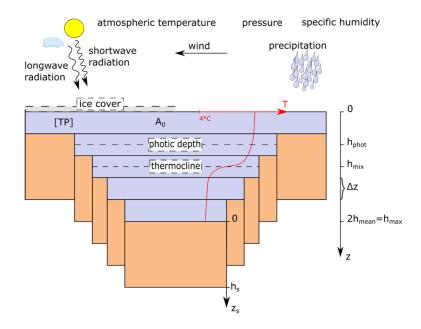


Fig. 2. Schematic representation of the lake morphology in FLaMe. The lake is represented by a "valley" shape (denoted by Eq. (1)). A_0 denotes the lake surface area, A is the area of each water layer, and h_{max} is the maximal water column depth. z represents the depth of a water column down to the surface of a sediment column while z_s stands for the depth inside a sediment column ($z_s = 0$ at the sediment water interface). The physical model is forced by longwave and shortwave radiation, near-surface wind, precipitation, atmospheric temperature, pressure, and specific humidity.

2.2.2 Biogeochemical Modules

2.2.2.1 Organic carbon module

Following the approach of Maavara *et al.* (2017), FLaMe does not resolve the vertical distribution of labile (i.e., microbial degradable) organic carbon (OC) concentrations ([$C_{OC,auto}$]) produced by inlake primary production, but only simulates the temporal dynamics of the volume-integrated autochthonous OC stock ($\overline{C_{OC,auto}}$, g C) (the overbar here indicates a volume-integrated value). $\overline{C_{OC,auto}}$





- should be understood as a simple indicator or an overall reflection of the resulting lake trophic status,
- 216 itself controlled by the combined effects of climate and nutrient loads from the catchment. The
- 217 allochthonous C inputs delivered from surrounding catchments are more refractory and thus perform
- as less important substrates for CH₄ production (Guillemette et al., 2017; DelSontro et al., 2018).
- 219 Thus, the autochthonous primary production is considered as the only labile OC source, neglecting
- the allochthonous OC contribution in this first version of FLaMe.
- The temporal evolution of volume-integrated labile OC stock is determined by the interplay
- 222 between autochthonous primary production, pelagic and benthic mineralization and burial fluxes
- 223 (Maavara et al., 2017):

$$\frac{\partial \overline{C_{OC,auto}}}{\partial t} = \overline{F_{PP}} - \overline{F_{Min}} - \overline{F_{Bur}}$$
 (2)

- 225 where t is time (day), and $\overline{C_{OC,auto}}$ is the volume-integrated OC stock (g C). $\overline{F_{pp}}$, $\overline{F_{Min}}$ and $\overline{F_{Bur}}$ are
- 226 the volume-integrated primary production, mineralization, and sedimentary burial fluxes (g C d-1),
- 227 respectively. Following Maavara et al. (2017), we assume that autochthonous primary production
- 228 rates are controlled by the light regime, water temperature, and the lake total dissolved phosphorus
- 229 (TDP) concentration ([TDP], g P m⁻³) (Reynolds, 2006). The volume-integrated $\overline{F_{PP}}$ can then be
- expressed using a classical Michaelis-Menten formulation (Mavaara et al., 2017):

$$\overline{F_{PP}} = B P_{Chl,max} M(T_{mean}) \frac{[TDP]}{K_{s,P} + [TDP]} V_{phot}$$
(3)

- where B is the phytoplankton biomass (expressed as chlorophyll-a concentration, g Chl-a m^{-3}) in the
- photic zone (Eq. (5)), $P_{Chl,max}$ is the maximum carbon fixation rate per unit of chlorophyll-a (g C (g
- 234 $Chla^{-1} h^{-1}$), M is a dimensionless metabolic correction factor that depends on the mean lake water
- temperature in photic zone T_{mean} (°C) (see Eq. (4)), $K_{s,P}$ is the half-saturation constant for phosphorus





- limitation (g P m⁻³), and V_{phot} is the water volume above the photic depth (m³). Parameters $P_{Chl,max}$
- and $K_{s,P}$ are constrained based on published observations (see section 2.3), while the metabolic factor
- 238 *M* is given by:

as:

239
$$M(T_{\text{mean}}) = \begin{cases} 1, & T_{\text{mean}} \ge 28^{\circ} \text{C} \\ Q_{10, prod}^{\frac{T_{\text{mean}} - 28}}{10}, & T_{\text{mean}} < 28^{\circ} \text{C} \end{cases}$$
 (4)

- 240 where $Q_{10,prod}$ is the temperature sensitivity for primary production, quantifying the increases of the
- 241 metabolic factor per 10 degree increase in temperature. Surface water phytoplankton biomass, B, is
- 242 approximated by a function of the photosynthetically active radiation (PAR), which is determined
- by shortwave radiation and light extinction in the water column:

244
$$B = \left(\frac{1}{k_c}\right) \left(0.75 \left(\frac{PP}{RP}\right) \ln \left(\frac{0.7PAR_0}{0.5PAR_b}\right) \left(\frac{1}{h_{prod}}\right) - \left(K_{dw} + K_{dp} + K_{dg}\right)\right)$$
 (5)

where k_c is the absorbance of PAR per unit of chlorophyll-a (m² (g Chl-a)⁻¹), and PP/RP is the ratio 245 246 of maximum gross photosynthesis to respiration per unit chlorophyll-a. PAR_0 is the PAR at the lake surface (µmol m⁻² s⁻¹), determined by the incoming shortwave radiation, as well as the daytime that 247 248 is specified by lake latitude and phenology (represented by the day of the year). PAR_k is the PAR at 249 the onset of photosaturation (μ mol m⁻² s⁻¹). The productive depth h_{prod} is determined as the 250 maximum of the thermocline and the photic depth simulated by the physical model. K_{dw} , K_{dp} , and 251 K_{dg} represent nonalgal PAR attenuations, due to pure water, inorganic suspended particulate matter, and labile carbon, respectively. Following Lewis (2011), K_{dg} is calculated as a function of $[C_{OC,auto}]$ 252

$$ln(K_{dg}) = -4.44 + 1.80ln([C_{OC,auto}]) - 0.149(ln([C_{OC,auto}]))^{2}.$$
 (6)





- Eq. (5) was derived based on the assumption of a balance between production and respiration (Reynolds, 2006; Lewis, 2011). Here we slightly relax this assumption and assume near-equilibrium conditions for given climate conditions at the monthly timescale, allowing us to simulate seasonal variations of primary production and associated biogeochemical processes. Note that this
- assumption is only used for biogeochemical variables related to primary production, while physical
- variables simulated by CSLM are resolved at a sub-daily time step.
- Following Hanson et al. (2011; 2014) and Maavara et al. (2019), the volume-integrated
- 262 mineralization rate is simulated as a function of temperature and labile OC availability:

$$\overline{F_{Min}} = k_{20} \,\theta^{T_{mean}-20} \,\overline{C_{OC,auto}} \tag{7}$$

- where k_{20} is a first-order rate constant for the mineralization of $\overline{C_{labile}}$ at 20 °C (d⁻¹). T_{mean} is the
- 265 mean water temperature (°C) in photic zone, and θ is the temperature dependence of mineralization
- of organic matter (Hanson et al., 2014).
- Following Maavara et al. (2019), the burial flux $\overline{F_{Bur}}$ is represented by a first order process
- 268 driven by the labile OC stock $\overline{C_{OC,auto}}$:

$$\overline{F_{Bur}} = k_{bur} \overline{C_{OC,auto}}$$
 (8)

- where k_{bur} is the burial rate constant and here set as half of the mineralization rate constant following
- 271 the ratios between these two processes reported in the global lake dataset (n=230) assembled by
- 272 Mendonça et al. (2017). This ratio is likely an upper bound because it accounts for contributions of
- 273 both autochthonous and allochthonous carbon sources in the dataset, while allochthonous inputs





should have distinct (but unquantified) ratios from autochthonous ones (Mendonça *et al.*, 2017; Guillemette *et al.*, 2017).

2.2.2.2 Methane module

The methane module simulates the dynamics of CH₄ concentration in both sediment and water columns as controlled by benthic CH₄ production, aerobic CH₄ oxidation, and diffusive and ebullitive transport from sediment to water and atmosphere (Fig. 3). Since the observational evidence suggests that benthic CH₄ production is the dominant CH₄ source in lakes (Tan *et al.*, 2015; Bastviken, 2022), we neglect the CH₄ production within the lake's water column in the model.

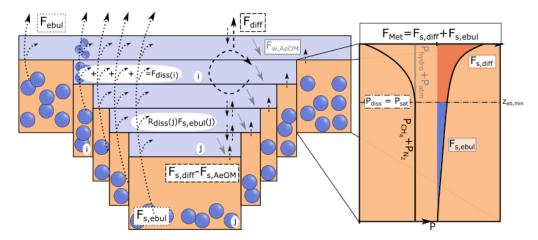


Fig. 3. Illustration of the methane (CH₄) module of FLaMe with a zoom into benthic CH₄ dynamics (zoom modified from Langenegger *et al.*, 2019). Benthic CH₄ production (zoom) assumes an exponential decrease in CH₄ production rate (F_{Met}) with depth. The CH₄ and N₂ partial pressures ($P_{CH4} + P_{N2}$) is mainly driven by the CH₄ production and follows the black curve profile, which starts to exceed the sum of the hydrostatic and atmospheric pressure ($P_{hydro} + P_{atm} - P_{H2O}$, grey line) at $z_{eb,min}$. Thus, this depth ($z_{eb,min}$) divides F_{Met} into a diffusive ($F_{s,diff}$, red filled region) and an ebullitive ($F_{s,ebul}$, cyan filled region) flux. $F_{s,AeOM}$ and $F_{w,AeOM}$ are the CH₄ oxidation in the





- sediment and water column, respectively. F_{diss} is the dissolution of the gas bubbles during transport through the water column. F_{diff} and F_{ebul} are diffusive and ebullitive CH₄ fluxes through the water-air interface, respectively.
- Within the lake sediment, CH₄ dynamics are determined by the balance between CH₄ production via methanogenesis and CH₄ migration to the water column through diffusive and ebullitive transport:

$$\frac{\partial \widetilde{CH_{4,s}}(z)}{\partial t} = \widetilde{F_{Met}(z)} - \widetilde{F_{s,diff}(z)} - \widetilde{F_{s,ebul}(z)} \tag{9}$$

$$\widetilde{F_{Met}(z)} = f_{mm} \frac{M_{CH4}}{M_C} \overline{F_{Min}} \frac{V_s(z)}{V_{s,tot}}$$
(10)

where the tilde overbar here represents the volume-integrated stocks or fluxes in the sediment column, which is different from the straight overbar for volume-integrated values in the water column. Note that we have sediment columns at different water depths, such that the stocks and fluxes are represented as a function of water depth z, which is characterized by the valley-shape model set-up and different from the conventional bucket shape set-up. $\widetilde{CH_{4,s}}(z)$ is thus the volume-integrated CH₄ stock for the sediment column with the sediment-water interface positioned at depth z (g CH₄). $\widetilde{F_{Mer}}(z)$ is the volume-integrated flux of CH₄ production through the entire sediment column with a sediment-water interface at depth z (g CH₄ d⁻¹), and $\widetilde{F_{s,ebul}}(z)$ and $\widetilde{F_{s,ebul}}(z)$ are volume-integrated diffusive and ebullition fluxes (g CH₄ d⁻¹) through the sediment-water interface at depth z, respectively. f_{mm} denotes the fraction of organic matter mineralization that proceeds via methanogenesis according to data compiled by Hanson $et\ al.$ (2014) and Bastviken (2022). M_{CH4}/M_{C} is a conversion factor corresponding to the molar ratio of CH₄ to $C_{OC,auto}$. As $f_{mm} \frac{M_{CH4}}{M_C} \overline{F_{Min}}$ is the total CH₄ production flux integrated over the whole water column, we assume that the fractions of





- 309 CH₄ production occurring in different sediment columns are set according to their volume
- 310 proportions, i.e., $\frac{V_s(z)}{V_{s,tot}}$.
- The partitioning of CH₄ production into ebullitive and diffusive fluxes depends on the porewater
- 312 CH₄ concentration or its partial pressure, which relies mainly on the vertical distribution of CH₄
- 313 production rate in the sediment as well as the oxygen concentration (but is of second-order
- importance). Based on the observation-based assumption that the organic carbon concentration and
- 315 thus mineralization rates exponentially decrease with sediment depth, we here assume an
- 316 exponentially decreasing relationship between methanogenesis rate versus depth (Fig. 3), following
- 317 Langenegger et al. (2019):

$$f_{met}(z, z_s) = F_{Met, 0}(z) \exp(-\alpha z_s)$$
 (11)

- where $f_{met}(z,z_s)$ is the methanogenesis rate (g CH₄ m⁻³ d⁻¹) at sediment depth z_s for the sediment
- 320 column with the sediment-water interface positioned at depth z. $F_{Met,0}(z)$ is the maximum CH₄
- 321 production at the sediment-water interface (g CH₄ m⁻³ d⁻¹) at depth z, and α is a shape parameter
- 322 (m⁻¹) that controls the decrease of methanogenesis rate with depth. As the shape of this curve
- 323 typically depends on the flux of labile carbon settling on the lake bottom, and thus, lake trophic
- status, the parameter α is here scaled by the F_{PP} empirically:

$$\alpha = \alpha_{min} + \beta \cdot F_{PP} \frac{V_w}{V_{phot}}$$
 (12)

- 326 where α_{min} is the minimum or base value, and β is the dependence of α on F_{PP} . The values of α_{min}
- 327 and β are determined based on the measurements in lakes of different trophic status reported by
- 328 Langenegger et al. (2019).





To determine the maximum CH₄ production $F_{Met,0}(z)$, the integral of CH₄ production rate over sediment column should equal to the volume-integrated CH₄ production flux $\widetilde{F_{Met}(z)}$ as specified by Eq. (10):

$$A_s(z) \int_0^{h_s} f_{met}(z, z_s) dz_s = \widetilde{F_{Met}(z)}$$
(13)

where $A_s(z)$ is the surface area of sediment column in contact with the water layer at lake depth z and is determined by difference in the areas of two adjacent water layers A(z) (Eq. (1)). The maximum CH₄ production at depth z, $F_{Met,0}(z)$, can be obtained by combining Equations (10), (11) and (13):

$$F_{Met,0}(z) = \frac{\overline{F_{Met}(z)}}{A_S(z)} \frac{\alpha}{1 - \exp(-\alpha h_S)}$$
 (14)

Since CH₄ production increases the *in-situ* CH₄ concentration as the sediment depth increases, the CH₄ concentration may exceed its solubility concentration and methane gas bubbles may start forming (Fig. 3). To constrain the partitioning of CH₄ production between diffusion and ebullition, the threshold sediment depth, $z_{\text{cb,min}}$, at which CH₄ concentration starts to exceed the solubility limit, is determined based on the equilibrium pressure condition following Langenegger *et al.* (2019) (see details in Supplementary Text S2). In the upper portion of the sediment column ($z_s < z_{\text{eb,min}}$), the produced CH₄ will diffuse into water; however, a fraction of the diffusing CH₄ will be oxidized in the transit through the upper sediment column, and only the remaining CH₄ will reach the sedimentwater interface. The volume-integrated CH₄ oxidation in the sediment at depth z, $F_{s,AeOM}(z)$, is here assumed to be controlled by the O₂ concentration in the overlying bottom water, and is represented by a Michaelis-Menten function:





$$\widetilde{F_{s,AeOM}}(z) = \widetilde{F_{Met}}(z) \frac{[O_2]_z}{K_{s,O} + [O_2]_z}$$
(15)

- 351 where $K_{s,O2}$ is the half-saturation constant of O_2 for the sedimentary CH₄ oxidation. As a result, the
- diffusive flux passing through the sediment-water interface is determined as follows:

353
$$\widetilde{F_{s,diff}}(z) = A_s(z) \int_0^{z_{eb,min}} F_{Met,0}(z) \exp(-\alpha z_s) dz_s - \widetilde{F_{s,AeOM}}(z)$$
 (16)

- In the lower portion of the sediment column ($z_s > z_{\rm eb,min}$; where oversaturation occurs), the
- produced CH₄ feeds the ebullitive flux, with the volume-integrated value $\widetilde{F_{s,ebul}}(z)$ (g CH₄ d⁻¹) as
- 356 given by:

$$\overline{F_{s,ebul}}(z) = A_s(z) \int_{z_{eb,min}}^{h_s} F_{Met,\theta}(z) \exp(-\alpha z_s) dz_s$$
(17)

- Note that Equations. (16) and (17) implicitly imply that, at the monthly resolution of our model, the
- 359 CH₄ dynamics in the sediment is at steady state and all the CH₄ produced during this time interval
- 360 is either oxidized or released through the water column via diffusive and ebullitive pathways.

Pelagic, dissolved CH₄ diffuses in the water column and its concentration is determined by the

363 diffusive CH₄ flux passing through the sediment-water interface (acting as a source for each water

layer), by aerobic CH₄ oxidation in the water column, and by the re-dissolution of the ebullitive CH₄

365 fluxes during transit through the water column. The mass conservation equation of dissolved CH₄ is

366 then given by:

$$\frac{\partial [CH_4]_w}{\partial t} = \frac{\partial}{\partial z} \left(K_{diff} \frac{\partial [CH_4]_w}{\partial z} \right) + \widetilde{F_{s,diff}}(z) \frac{1}{A(z)dz} - F_{w,AeOM}(z) + F_{diss}(z)$$
(18)





where $[CH_4]_w$ is the pelagic CH_4 concentration (g CH_4 m⁻³) and K_{diff} is the eddy diffusion coefficient of CH_4 in water (m² d⁻¹). $F_{s,diff}(z) \frac{1}{A(z)dz}$ is the change of CH_4 concentration induced by diffusive inputs from the sediment columns, the term A(z)dz being the volume of the water layer connected to the corresponding sediment column. $F_{w,AeOM}(z)$ is the aerobic CH_4 oxidation rate in the water column, and is described through double Michaelis-Menten reaction kinetics (Stepanenko *et al.*, 2016; Liikanen *et al.*, 2002; Thottathil and Prairie, 2019):

374
$$F_{w,AeOM}(z) = k_{max} Q_{10,ox}^{\frac{T-T_r}{10}} \frac{[CH_4]_{w,z}}{K_{s,CH_4} + [CH_4]_{w,z}} \frac{[O_2]_z}{K_{s,O_2} + [O_2]_z}$$
(19)

- where k_{max} is the maximum CH₄ oxidation rate (Liikanen et al. 2002), T is the water temperature, T_r is the reference temperature, and $Q_{10,ox}$ expresses the temperature dependency of the CH₄ oxidation rate. $K_{s,CH4}$ and $K_{s,O2}$ are the half-saturation constants for CH₄ and O₂, respectively.
- To constrain the redissolution of gas bubbles ($F_{diss}(z)$), we follow the approach proposed by
 McGinnis *et al.* (2006) where a function ($f_{bdiss}(z)$) is used to represent the fraction of the benthic
 ebullitive CH₄ flux that redissolves in the water column during gas ascent. This fraction is a function
 of water depth and gas bubble diameter, and the latter was set to 5 mm following Delwiche and
 Hemond (2017). With this function $f_{bdiss}(z)$, the redissolved CH₄ fluxes from sediment column at
 depth z are assumed to be evenly redistributed in the water layers above the sediment, i.e.,

$$f_{rediss}(z) = \frac{f_{bdiss}(z)F_{s,ebul}(z)}{\int_0^z A(z)dz}$$
 (20)

where $\int_0^z A(z)dz$ is the water volume above the sediment layer at the depth of interest z. Then, at this particular depth z, the redissolution flux $(F_{diss}, g \text{ CH}_4 \text{ m}^{-3} \text{ d}^{-1})$ is thus determined as follows:

$$F_{diss}(z) = \int_{z}^{h_{max}} f_{rediss}(z) dz$$
 (21)





- where $\int_{z}^{h_{max}} f_{rediss}(z) dz$ represents the integral of all re-dissolved ebullitive fluxes from sediment columns below z.
- By deducing this dissolution flux from the ebullitive flux released from lake sediments, the resultant ebullitive flux reaching the atmosphere (F_{ebul} ; g CH₄ m⁻² d⁻¹) is calculated as:

$$F_{ebul} = \frac{1}{A_0} \int_0^{h_{max}} \left(1 - f_{bdiss}(z) \right) \widetilde{F_{s,ebul}}(z) dz$$
 (22)

- where A_0 is the lake surface area, and $\left(1-f_{bdiss}(z)\right)\widetilde{F_{s,ebul}}(z)$ is the component of ebullitive flux at depth z that reaches the atmosphere.
 - In addition to diffusive and ebullitive pathways, FLaMe also calculates a storage flux (F_{stor}) that encapsulates the changes in the total CH₄ mass stored in hypolimnion due to the weakening of lake stratification or turnover events when the lake surface temperature crosses the threshold of 4°C (MacKay, 2012; MacKay *et al.*, 2017). This results in a full mixing of the lake that releases the previously accumulated CH₄ in the anoxic portion of the lake and concomitantly fully aerates the water column. Lake turnovers thus lead to a complete homogenization of O₂ and CH₄ concentration across the vertically resolved water column. Upon full mixing, remobilization of larger CH₄ stocks that accumulated in the hypolimnion abruptly increase the CH₄ concentration near the lake surface, and hence strongly enhance the diffusive flux through the air-water interface. That is, the storage flux in FLaMe is not simulated separately but it is implicitly incorporated into the diffusive flux $F_{\rm diff}$ which increases dramatically following the formation of a very sharp CH₄ concentration gradient at the lake surface.





2.2.2.3 Oxygen module

The oxygen module is needed to simulate the lake methane processes (section 2.2.2.2). It represents the O₂ cycle within the water column, driven by O₂ production by photosynthesis, O₂ consumption by pelagic and benthic OC mineralization, and aerobic pelagic and benthic CH₄ oxidation. These processes are coupled to the vertical diffusive transport of O₂ through water column (Fig. 4). The one-dimensional conservation equation for O₂ concentration in the water column is thus given by:

414
$$\frac{\partial[O_2]}{\partial t} = \frac{\partial}{\partial z} (K_{diff} \frac{\partial[O_2]}{\partial z}) + OF_{PP}(z) - OF_{w,Aer}(z) - \frac{1}{A(z)dz} \widetilde{OF}_{s,Aer}(z) - OF_{w,AeOM}(z) - OF_{s,AeOM}(z)$$
 (23)

415 where $[O_2]$ is the O_2 concentration in the water (g O_2 m⁻³), and K_{diff} is the eddy diffusion coefficient 416 of O_2 (m² d⁻¹), assumed identical to that of CH₄. $OF_{PP}(z)$ is the oxygen production through primary 417 production (g O_2 m⁻³ d⁻¹) at depth z. $OF_{w,Aer}(z)$ is the O_2 consumption by heterotrophic respiration 418 (g O₂ m⁻³ d⁻¹) in the water column at depth z, while $\widetilde{OF}_{s,Aer}(z)$ is the volume-integrated O₂ 419 consumption by heterotrophic respiration in the sediment (g O_2 m⁻³ d⁻¹), and A(z)dz is the volume 420 of the water layer connected to the corresponding sediment column. $OF_{w,AeOM}(z)$ and $OF_{s,AeOM}(z)$ are the aerobic CH₄ oxidation in the water column and sediment (g O₂ m⁻³ d⁻¹), respectively, at depth 421 422 z.





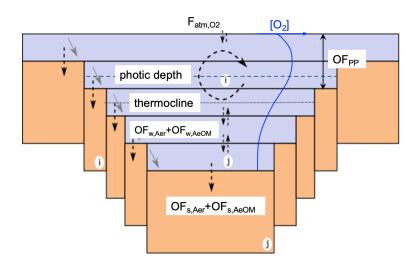


Fig. 4. Illustration of the oxygen (O₂) module in the FLaMe model. The O₂ production due to primary production occurs only in the photic zone (OF_{PP}), while the O₂ consumption by heterotrophic respiration occurs in both the entire pelagic zone and benthic zone (OF_{w,Aer} and OF_{s,Aer}). The O₂ consumption due to CH₄ oxidation occurs also in both pelagic and benthic zones (OF_{w,AeOM} and OF_{s,AeOM}). In this figure, the dotted arrows crossing the sediment-water interface represent the O₂ demands in sediments (OF_{s,Aer} and OF_{s,AeOM}), the dashed arrows represent the eddy diffusion of O₂ between water layers and through the water-air interface, and the tilted grey arrows represent the aerobic oxidation of CH₄ in the water column. As a result, the blue curve depicts a typical vertical profile of O₂ concentration under lake water stratification.

Photosynthesis occurs only in the photic zone, and the amount of O_2 produced by primary production $\overline{OF_{PP}}$ (volume-integrated value; g O_2 d⁻¹) can be determined according to the stoichiometric ratio M_{O2}/M_C , where and M_{O2} and M_C are the molar masses of oxygen and carbon, respectively. To resolve the vertical O_2 profile, the O_2 produced during primary production is assumed to be evenly redistributed within the water layers above the photic depth (Fig. 4):





$$OF_{PP}(z) = \begin{cases} \overline{F_{PP}} \frac{1}{V_{phot}} \frac{M_{O_2}}{M_C}, & z < z_{phot} \\ 0, & z \ge z_{phot} \end{cases}$$
(24)

- 438 where V_{phot} is the photic volume.
- The oxygen consumption induced by CH₄ oxidation in the sediment and water column can be
- calculated from corresponding CH₄ fluxes (Eqs. (15) and (19), respectively) and the stoichiometry
- 441 of the reactions involved:

442
$$OF_{s,AeOM}(z) = \frac{2M_{O_2}}{M_{CH_4}} F_{s,AeOM}(z)$$
 (25)

$$OF_{w,AeOM}(z) = \frac{2M_{O_2}}{M_{CH_4}} F_{w,AeOM}(z)$$
 (26)

- As in Eq. (10), a fraction of the mineralized organic carbon (represented by f_{mm}) is channeled
- 445 into the methanogenesis pathway according to the data compiled by Hanson et al. (2014) and
- Bastviken (2009). Thus, the remaining fraction $(1-f_{mm})$ of the total mineralization $\overline{F_{Min}}$ is channeled
- 447 into the aerobic metabolic pathway (F_{Aer}) . As a result, the bulk volumetric rate of oxygen
- 448 consumption due to the aerobic metabolic activity (OF_{Aer}) can be represented by the fraction $1-f_{mm}$
- and the volume-integrated mineralization $\overline{F_{Min}}$:

$$OF_{Aer} = (1 - f_{mm}) \overline{F_{Min}} \frac{1}{V_{vo}} \frac{M_{O2}}{M_C}$$

$$(27)$$

- 451 In the sediment, the aerobic mineralization occurs only in the upper oxic layer. The thickness
- 452 of this aerobic layer is limited by the oxygen penetration depth zox. Following Ruardij and Van
- 453 Raaphorst (1995), this depth z_{ox} can be derived by solving the steady-state reaction-diffusion
- 454 equation for O₂ in the sediment:

$$z_{ox} = \sqrt[2]{\frac{2K_{s,diff}}{OF_{s,AeOM} + OF_{Aer}}}$$
 (28)





- where $K_{s,diff}$ is the molecular diffusion coefficient within the sediment, which is dependent on the
- 457 temperature (Ruardij and Van Raaphorst, 1995). The amount of O₂ consumed within the oxic layers
- of the sediment can thus be determined as:

$$\widetilde{OF_{s,Aer}}(z) = OF_{Aer}A_s(z)z_{ox}$$
(29)

- 460 where $A_s(z)$ is the area of the corresponding sediment column at depth z. To ensure a mass balance,
- 461 the volumetric rate of O₂ consumption due to aerobic metabolism in water can then be calculated
- as follows:

$$OF_{w,Aer}(z) = OF_{Aer} - O\widetilde{F_{s,Aer}(z)} \frac{1}{A(z)dz}$$
(30)

- where A(z)dz is the volume of the water layer connected to the corresponding sediment column, and
- 465 it is used here to convert the sedimentary O₂ consumption into a volumetric rate in the water column.
- 466 Furthermore, following Martin et al. (1987), Carlson et al. (1994) and Aristegui et al. (2003), we
- 467 redistribute the respiration $(OF_{w,Aer})$ within the water column, assuming that 80% of the respiration
- 468 occurs in the photic zone, with the remaining 20%, sustained by the export production, occurs in the
- deeper water layers where it can further degrade.

2.2.3 Boundary conditions for the transport module

- The partial differential equations (18) and (23) require boundary conditions to constrain the diffusive transport (i.e., the first term on the right-hand side of both equations). At the sediment-
- 473 water interface, a zero-flux boundary condition is imposed, because the diffusive exchanges of CH₄
- 474 and O₂ between the sediment columns and the overlying waters are already included as source/sink
- 475 terms in Eq. (18) and (23). This choice was guided by the valley-shape configuration of our lake set-
- 476 up, and thus by the presence of diffusive CH₄ and O₂ exchange fluxes with sediment in each water





- layer of our model, a situation in stark contrast from a bucket shape model where only a single
- sediment column would be connected to the bottom water layer.
- At the lake surface (z = 0 m), the boundary conditions are determined by the CH₄ and O₂
- exchange fluxes with the atmosphere, as given by (Wanninkhof et al., 2009; Cole and Caraco, 1998):

481
$$F_{\text{atm,CH}_4} = k_{ge}([\text{CH}_4] - f_{CH4,atm} P_{\text{atm}} M_{CH4} K_{H,CH4} \exp(\frac{\partial \ln(K_{H,CH4})}{\partial \frac{1}{T_I}} (\frac{1}{T_I} - \frac{1}{298.15})))$$
(31)

482
$$F_{\text{atm,O}_2} = k_{ge}([O_2] - f_{O2,atm} P_{\text{atm}} M_{O2} K_{H,O2} \exp(\frac{\partial \ln(K_{H,O2})}{\partial \frac{l}{T}} (\frac{1}{T_I} - \frac{1}{298.15})))$$
(32)

- 483 where $F_{\text{atm},CH4}$ and $F_{atm,O2}$ are diffusive fluxes of CH₄ (g CH₄ m⁻²d⁻¹) and O₂ (g O₂ m⁻² d⁻¹) through
- the air-water interface of the lake, respectively. f_{CH4,atm} and f_{O2,atm} are molar fractions of CH₄ and O₂
- in the atmosphere, respectively, and P_{atm} is the atmospheric pressure. $K_{H,CH4}$ and $K_{H,O2}$ are Henry's
- 486 constants of CH₄ and O₂ at 298.15 K and $k_{\rm ge}$ is the piston velocity (m s⁻¹), here constrained from the
- 487 empirical equation reported by Cole and Caraco (1998), as in Tan et al. (2015; 2018) and Stepanenko
- 488 et al. (2016):

$$k_{ge} = (C_{k_I} + C_{k_2} v_{a,10}^n) \sqrt{\frac{600}{S_{CX}}}$$
(33)

- where C_{k1} , C_{k2} and n are empirical constants (Cole and Caraco, 1998). $v_{a,10}$ is the absolute wind
- 491 velocity measured at 10 m above the lake surface (m s⁻¹), and $S_{c,CH4}$ and $S_{c,O2}$ are the Schmidt number
- 492 of CH₄ and O₂, respectively (Wanninkhof et al. 2009). Note that more recently new formulations of
- $k_{\rm ge}$ have been proposed (McIntire et al., 2020) but we here choose to use Eq. (33) following previous
- 494 modelling studies (Tan et al., 2015; Stepanenko et al. 2016; Tan et al., 2018).





496

497

498

499

500

501

502

503

504

505

506

507

508

509

510

511

512

513

514

515

516

2.3 Parameter values

Table 1 summarizes all physical and biogeochemical parameters, their values, as well as the original references from which they were extracted. Most of these parameters were either directly taken from relevant modelling studies or constrained based on comprehensive literature reviews. In addition, several key parameters of the FLaMe model, highlighted in Table 1, were adjusted by calibrating the model based on observations of lake C fluxes (i.e., F_{PP}, diffusive and ebullitive CH₄ emissions). For instance, the parameters $P_{\text{Chl,max}}$ and $K_{s,P}$ control the lake primary production and were tuned to reproduce broad global patterns of primary production rates across the full range of lake trophic status (Wetzel, 2001). The mineralization k_{20} and burial constants k_{bur} were adjusted based on the observed fraction of Coc, auto that settles onto the lake sediment, either to be decomposed in anerobic or oxic conditions or accumulated in the sediment (Hanson et al., 2011, 2014; Maavara et al., 2019; Mendonça et al., 2017). The temperature dependence of mineralization θ was finetuned to reproduce the observational ranges of temperature dependence of net-CH₄ emissions (Aben et al., 2017). f_{mm} specifies the fraction of mineralization that channels to the methanogenesis pathway, which is adjusted to produce the observational patterns of CH₄ emissions. α_{min} is the base value of the exponentially decreasing rate of CH₄ production versus sediment depth, and controls the split of CH₄ production between diffusive and ebullitive pathways, which was calibrated to reproduce observed broad trends of F_{tot} , F_{ebul} and F_{diff} from the literature (Rinta et al., 2017). The parameter values listed in Table 1 provide the reference setup for the simulation of lake CH₄ emissions, and the sensitivity and uncertainty analyses regarding the key model parameters (listed in Table 3) is carried out using wide ranges of values covering most possible lake conditions from the real world (see section 3.3.3).



521

522

523

524



2.4 Numerical solution

518 In FLaMe, the physical (i.e., CSLM) and biogeochemical (OC, CH₄ and O₂) modules are 519 coupled online. For the dynamics of volume-integrated OC and CH4 in sediments, the involved 520 ordinary differential equations are solved using a forward Euler scheme. For the dynamics of dissolved O2 and CH4 concentrations in the water column, the partial differential equations (Eqs. (18) and (23)) are solved numerically using an explicit central difference scheme for depth and Euler forward scheme for time. The diffusion coefficient Kdiff for both O2 and CH4 is depth dependent (Table 1) to capture the reduced transport when the temperature gradient from the epilimnion, 525 metalimnion and hypolimnion is well pronounced (Dong et al. 2020; Imboden and Wuest 1995; 526 Imberger 1985; Boehrer and Schultze 2008).





527 Table 1. Model parameters of FLaMe v1.0 and the choice of their values

Main processes	cesses parameters see s Steepness of lakebed (-)		Values	Equations	References
Lake morphology			2	(1)	-
Primary production	$P_{ m chl,max}$	Maximum carbon fixing rate per unit of Chlorophyll-a (mg C (mg Chl-a) ⁻¹ h ⁻¹)	0.5*	(3)	Behrenfeld and Falkowski (1997)
	$K_{ m s,P}$	Half saturation coefficient of 0.09* total dissolved phosphorus for the primary production (g m ⁻³)		(3)	Maavara et al., (2017)
	Q10,prod	Temperature sensitivity for the primary production	2	(4)	Lewis (2001) and Reynolds (2006)
	k_c	Absorbance of PAR per unit of chlorophyll-a (m² (g Chl-a)-1)	0.014× 10 ³	(5)	Lewis (2001) and Reynolds (2006)
	PP/RP	ratio of maximum gross photosynthesis to respiration per unit chlorophyll-a (-)	15	(5)	Lewis (2001) and Reynolds (2006)
	PAR_k	PAR at the onset of photo saturation (μmol m-2 s-1)	120	(5)	Lewis (2001) and Reynolds (2006)
	K_{dw}	PAR attenuations due to pure water	0.13	(5)	Lewis (2001) and Reynolds (2006)
	K_{dp}	PAR attenuations due to suspended particulate matter	0.06	(5)	Lewis (2001) and Reynolds (2006)
Mineralization and burial of organic	k_{20}	Mineralization rate at a reference temperature of 20 °C (d ⁻¹)	0.008*	(7)	Maavara <i>et al.</i> , (2017)
carbon	θ	Temperature dependence of mineralization	1.02*	(7)	Maavara <i>et al.</i> , (2017)





	$k_{ m bur}$	Carbon burial rate in the lake (d^{-1})	0.004*	(8)	Mendonca <i>et al.</i> , (2017)
	fmm	Fraction of mineralization that channels to the methanogenesis pathway	1/4*	(10) and (27)	Hanson <i>et al.</i> (2014); Bastviken (2009)
CH ₄ oxidation	k _{max}	Maximal rate of CH ₄ oxidation (g CH ₄ m ⁻³ d ⁻¹)	0.69	(19)	Liikanen et al. (2002)
	Q10,0x	Temperature dependence of CH ₄ oxidation (-)	1.2	(19)	Liikanen et al. (2002)
	K _{s,CH4}	Half-saturation constant for CH ₄ (g CH ₄ m ⁻³)	0.6	(19)	Stepanenko et al. (2016)
	$K_{s,O2}$	Half-saturation constant for O_2 (g O_2 m ⁻³)	0.67	(19)	Liikanen et al. (2002)
Shape parameter of sedimentary CH ₄ production	C _{min}	Base value of the exponentially decreasing rate of CH ₄ production versus sediment depth (m ⁻¹)	10*	(12)	Langenegger et al., (2019)
Gas transport in the water column and exchange with air	K_{diff}	Depth-dependent eddy- diffusion coefficient (m ² d ⁻¹)	8.64 (epilimnion), 8.64× 10 ⁻³ at	(18) and (23)	Stefan and Fang (1994)
exchange with			the termocline, and 8.64×10 ⁻¹ (hypolimnion)		
exchange with	C_{kl}	Empirical constant for piston velocity (m s ⁻¹)	termocline, and 8.64×10 ⁻¹	(33)	Cole and Caraco, (1998)
exchange with	C_{k1}		termocline, and 8.64×10 ⁻¹ (hypolimnion)	(33)	Caraco,
exchange with		velocity (m s ⁻¹) Empirical constant for piston	termocline, and 8.64×10 ⁻¹ (hypolimnion) 5.75×10 ⁻⁶		Caraco, (1998) Cole and Caraco,





$S_{c,O2}$	Schmidt number of O ₂ (-)	589	(33)	Wanninkhof et al. (2009)	
fCH4,atm	Atmospheric molar fractions of CH ₄	0.18×10 ⁻¹³	(31)	Lan <i>et al.</i> (2024)	
f02,atm	Atmospheric molar fractions of O ₂	0.2095	(32)	Gatley <i>et al.</i> (2008)	

^{*} indicates that the original parameter values are from the literature, and further adjusted by calibration

⁵²⁹ versus observations.





2.5 Case studies

We implemented three case studies to assess the performance of FLaMe in simulating lake CH₄ emissions, as well as its application to the European scale. First, we present theoretical simulations for two representative cases (methodological details in section 2.5.1) to assess the general behaviors of FLaMe in capturing the physical-biogeochemical patterns of contrasted lakes. Then, we perform the simulations for four well-surveyed real lakes to assess the model's capability in capturing the observed temporal variations of CH₄ fluxes (section 2.5.2). Next, we apply FLaMe to the entire European domain to assess the model's capability in reproducing the spatial patterns and seasonal variations of CH₄ fluxes at continental scale (section 2.5.3). The European scale application can be considered as a "proof of concept" in support of our proposed modeling strategy. Finally, we examine the sensitivity to key model parameters and assess the uncertainty of the continental-scale emissions using the samples produced by sensitivity analysis, combined with a machine learning approach (section 2.5.4).

2.5.1 Two theoretical representative lakes for testing FLaMe performance

To test if the FLaMe model can capture the contrast in physical-biogeochemical behaviors across shallow vs. deep, eutrophic vs. oligotrophic and warm vs. cold lakes, we set-up the model for two theoretical representative lakes: a "deep oligotrophic" lake (h_{max} = 35 m or h_{mean} = 17.5 m and [TP] = 3 μ g P L⁻¹) driven by a "cold" climate (63.75°N, 26.25°E; Fig. S1) and a "shallow eutrophic" lake (h_{max} = 10 m or h_{mean} = 5 m and [TP] = 80 μ g P L⁻¹) driven by a "warm" climate (43.75°N, -6.25°E; Fig. S2). For these two theoretical representative cases, FLaMe simulates the spatio-temporal evolutions of physical and biogeochemical variables and fluxes, including primary production and mineralization fluxes, and labile autochthonous OC stocks as well as the vertically resolved gradients





of temperature, CH₄ and O₂ concentrations. Furthermore, we also compared the seasonal patterns of CH₄ productions and emissions for these two contrast lakes. To investigate further how environmental factors affect the FLaMe model behavior, we further decompose the collective responses of shallow and deep lakes into individual effects induced by trophic level, climate (Fig. S1–S3) and lake depth using hypothetical numerical simulations, i.e., (i) changing the maximal lake depth (h_{max}) from 5 to 25 m; (ii) increasing the [TP] levels from 8 to 80 µg P L⁻¹; and (iii) changing the climate from warm (43.75°N, -6.25°E; Fig. S1) to cold conditions (63.75°N, 26.25°E; Fig. S2).

2.5.2 Simulations of temporal patterns for four well-surveyed lakes

To evaluate the ability of FLaMe to reproduce the observed temporal patterns of CH₄ fluxes, we selected four lakes from the Inter-Sectoral Impact Model Intercomparison Project (ISIMIP) lake datasets for which monthly resolved temporal CH₄ fluxes were available. These lakes cover different lake depths, areas, climate conditions and trophic statuses, as summarized in Table 2. Since *in-situ* measurements of climatic drivers are not available for these lakes, we extracted them from the 0.5°x0.5° GSWP3-W5E5 global climate forcings released by the ISIMIP3a project as an approximation. The measurements of CH₄ fluxes for these lakes were mostly collected during the first 20 years of the 21st century, and we thus selected the climate forcings for the period 1991–2019, using the period 1991–1999 as spin-up phase. Since the lack of *in-situ* measured climatic drivers, as well as observations of variations in lake water levels and areas, affect the model's ability to capture the full variability in the observed CH₄ emission time series, we here focus only on the magnitudes and broad seasonal patterns in observed CH₄ emissions. Thus, we evaluated the simulated statistics (mean and SD represented by boxplots) of CH₄ fluxes within the year against the observational data.





Table 2. Characteristic information for the four well-surveyed lakes from ISIMIP datasets

Lake	Coordinates	Lake depth	Lake area (km²)	Climate	Trophic status	Data
Klöntal	47.026N, 8.981E	21.4m (mean), 45m (max)	2.25	Temperate	Oligotrophic	Annual mean
Erssjön	58.371N, 12.162E	1.3m (mean), 4.75m (max)	0.062	Temperate- Boreal	Mesotrophic	2012–2013
Upper Mystic	42.434N, 71.150W	11.7m (mean), 25m (max)	0.58	Temperate	Eutrophic	2007–2008
Villasjön	68.35N, 19.03E	1.3 m (max)	0.17	Boreal	Oligotrophic	2010–2017

2.5.3 Implementation of FLaMe at continental scale

To implement the model at the scale of Europe (25°W–60°E, 36°–71°N), we extracted the lakes within this domain from the HydroLAKES database (Messager *et al.*, 2016; n=108407, total area = 1.33×10^5 km² for lakes with $0.1 \le A_0 \le 1000$ km² within the European domain). Following our clustering strategy, we subdivided, within each grid cell, all lakes into four classes based on their surface area ($0.1 \le A_0 \le 1$ km², $1 \le A_0 \le 10$ km², $10 \le A_0 \le 100$ km², and $100 \le A_0 \le 1000$ km²). As FLaMe was derived from the small lake physics model CSLM, we here only considered the lakes with an area smaller than 1000 km², and excluded the very large lakes ($A_0 \ge 1000$ km²) that account for 40% of the total European lake surface area (but only consist of 21 lakes). Within our model domain, we have 108407 lakes with a surface area larger than 0.1 km², which at spatial resolution of 2.5 degree (Fig. S4–S5) result in 365 grid cells and 953 representative lakes (hence reducing computation cost by more than a factor of 100 compared to a case where each individual lake would be simulated). By parallelizing the model simulations on a high-performance cluster, the implementation of FLaMe





for the entire European domain consumes approximately 365 CPU hours for a single run covering 10 years.

The FLaMe model was forced by meteorological conditions from the GSWP3-W5E5 reanalysis product under ISIMIP3a (Frieler *et al.*, 2024) (Fig. S6), including shortwave solar radiation (W m⁻²), longwave solar radiation (W m⁻²), precipitation (mm s⁻¹), near surface air temperature (at 10 m height, °C), specific humidity (kg kg⁻¹), near surface wind velocity (at 10m, m s⁻¹), and atmospheric pressure (Pa). As these forcings were provided at a finer spatial resolution of 0.5°, we only applied the values in the central 0.5° grid cell of our larger 2.5° grid. In addition, the FLaMe model was also driven by the TDP in the representative lakes (Fig. S7–S8), which was estimated by dividing the TDP mass outflow by the water discharge reported in HydroLAKES, hence assuming that the lake water is well mixed. The TP mass outflow from each lake in HydroLAKES was obtained by routing the TP loads (extracted from the GlobalNEWS model; Mayorga *et al.*, (2010)) from the watershed (point and non-point terrestrial sources) into the river network, following the procedure outlined in Lauerwald *et al.* (2019) and topological information provided by the HydroSHEDS drainage network. More details related to the TP routing can be found in Bouwman and Billen (2009), Van Drecht *et al.* (2009), and Mayorga *et al.* (2010).

2.5.4 Sensitivity and uncertainty analysis

To explore how model parameterization affects the European-scale assessments of lake CH₄ emissions, we conducted a sensitivity analysis encompassing the parameters whose variations induce the largest changes in lake CH₄ dynamics and listed in Table 3. The sensitivity was conducted by varying a parameter once at a time: only one parameter is varied with the other parameters kept





610 unchanged. All these parameters were assumed to have Gaussian distributions, with their SDs 611 specified as 50% of their original values, except the temperature dependency $Q_{10,\text{ox}}$ and θ whose 612 SDs were specified as 50% of their deviation to unity. More specifically, we tested the sensitivity 613 within the ranges of mean±SD at four points, i.e., +SD, +0.5SD, -0.5SD, and -SD. 614 To constrain uncertainties in European scale CH₄ emissions, we complemented the sensitivity 615 analysis (n=36) with another 28 scenarios under several extreme cases and different combinations 616 of variations in key parameters. With these 64 assessments taken as samples, we then used a machine 617 learning approach to assess the uncertainty associated to our estimation of European lake CH₄ fluxes. 618 Specifically, we trained a Random Forest (RF) model that capture nonlinear relationships between 619 our key model parameters and European lake CH₄ emissions, i.e., the key parameters are taken as 620 predictors and the European lake CH₄ emissions are taken as target variable. Next, we produced 621 1000 Gaussian-distributed random samples within the parameter space and estimated an ensemble 622 of CH₄ emissions using the trained RF model.





Table 3 Key model parameters selected for sensitivity and uncertainty analysis

Main processes	Key model parameters	Physical meanings (units)	Values	Ranges	Eq.	References
Primary production	$P_{ m chl,max}$	Maximum carbon fixing rate per unit of Chlorophyll-a (mg C (mg Chl-a) ⁻¹ h ⁻¹)	0.5	0.5–6	(3)	Behrenfeld and Falkowski (1997)
	$K_{\mathrm{s,p}}$	Half saturation coefficient of total dissolved phosphorus for the primary production (g m ⁻³)	0.09	0.006–0.189	(3)	Maavara <i>et al.</i> , (2017)
Mineralizat ion and burial of organic carbon	k ₂₀	Mineralization rate at a reference temperature of 20 °C (d ⁻¹)	0.008	0.003-0.015	(7)	Maavara <i>et al.</i> , (2017)
	θ	Temperature dependence of mineralization	1.02	1.01–1.07	(7)	Maavara <i>et al.</i> , (2017)
	$k_{ m bur}$	Carbon burial rate in the lake (d ⁻¹)	0.004	$1/2k_{20}$	(8)	Mendonca <i>et al.</i> , (2017)
	fmm	Fraction of mineralization that channels to the methanogenesis pathway	1/4	1/6–1/2	(10) (26)	Hanson <i>et</i> <i>al.</i> (2014); Bastviken (2009)
CH ₄ oxidation	k _{max}	Maximal rate of CH ₄ oxidation (g CH ₄ m ⁻³ d ⁻¹)	0.69	0.19–7.68	(18)	Liikanen et al. (2002)
	Q10,0x	Temperature dependence of CH ₄ oxidation (-)	1.2	1.1–2.0	(18)	Liikanen et al. (2002)
Base value of the shape parameter	$lpha_{min}$	Exponentially decreasing rate of CH ₄ production versus sediment depth (m ⁻¹)	10	10–70	(12)	Langenegge r et al., (2019)





3. Results

3.1 Assessing the performance of FLaMe in capturing patterns of CH₄ dynamics across

different lake types

The FLaMe model is shown to be able to well capture the typically observed, contrasting physical and biogeochemical behaviors for two representative cases (Fig. 5 and Fig. S9–17; more details in Supplementary Text S3): shallow vs. deep, eutrophic vs. oligotrophic and warm vs. cold lakes. In the deep oligotrophic lake, the mean temperature reveals a lower and narrower seasonal variability (\sim 3–8° C) compared to the shallow eutrophic lake (5–15°C) (Fig. 5a vs. 5b). Large temperature variations in the latter are mainly driven by the smaller water volume and thus faster mean temperature response to fluctuations in atmospheric temperature. In addition, the annual averaged F_{PP} in the shallow eutrophic lake (490 gC m⁻² yr⁻¹) is approximately 38 times higher than that in the deep oligotrophic lake (13 gC m^{-2} yr⁻¹) (Fig. 5c vs. 5d). This difference can be explained by the differences in water volume (energy exchange), trophic status, and climate forcings. The higher F_{PP} of the shallow eutrophic lake also translates into higher $C_{OC,auto}$ concentration (\sim 110 times) which persist over longer periods (Fig. 5e vs. 5f), despite substantially higher F_{min} rates.





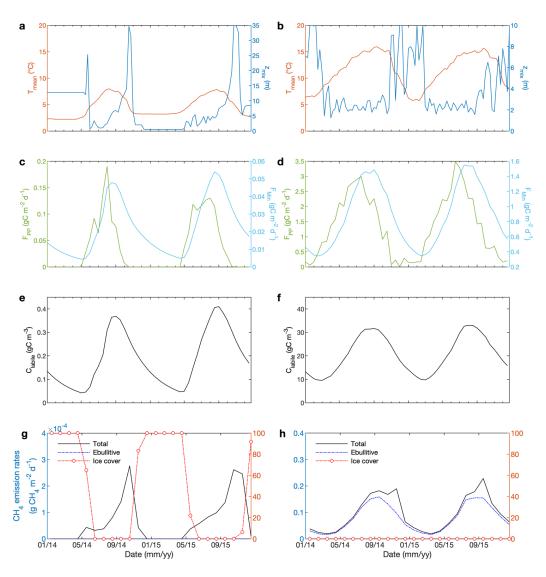


Fig. 5. Depth-integrated temporal evolution of variables and processes in two theoretical representative lakes. The deep oligotrophic lake (left) has a maximal depth of 35 m and [TDP] of 3 μ g 2 L $^{-1}$, and is driven by the climate forcings at the location of 63.75° 2 $^$



647

648

649

650

651

652

653

654

655

656

657

658

659

660

661

662

663

664

665

666



autochthonous organic carbon (C_{OC,auto}); (g) and (h) show the evolution of CH₄ emission rates and ice cover.

Note the difference scales between the left and right panels.

In the deep oligotrophic lake, the simulated vertical temperature profiles indicate an almost permanently maintained stratification that is only interrupted by short but intense turnover events during late falls (Fig. S9a). Lake stratification (e.g., lake turnover and O₂ concentrations that depend mostly on solubility and hence, temperature) dominates the spatio-temporal pattern of O2 such that O₂ concentration is near-saturated during most of the year (Fig. S9c). The oligotrophic status, together with the well oxygenated conditions, results in extremely low CH₄ concentrations. Higher CH₄ concentrations are only simulated near the lake bottom following the productive season, i.e., late summer/fall transition (Fig. S9e). In contrast, in the shallow eutrophic lake, the weaker stratification results in a less pronounced vertical temperature gradient (Fig. S9b). The vertical lake O2 profile is not only controlled by the lake physics (temperature and O2 solubility) but also by intense biogeochemical processes (Fig. S9d). During summer, O2 concentrations in the upper portion of the lake are slightly supersaturated due to photosynthetic activity, followed by a gradual decrease in O₂ concentration as mineralization rates exceed primary production rates. Due to the high primary production in the eutrophic lake, large amounts of OC are exported below the thermocline, where heterotrophic activity progressively depletes O2, leading to the development of anoxic conditions in the hypolimnion. The combination of high F_{Min} and low O_2 concentrations drive the accumulation of CH₄ in late summer at the bottom of the lake (Fig. S9f), with maximal CH₄ concentration (3.0 g CH₄ m⁻³) exceeding those simulated in the deep oligotrophic lake by a factor of 600 (Fig. S9e).



668

669

670

671

672

673

674

675

676

677

678

679

680

681

682

683

684

685

686

687

688



By aggregating CH₄ fluxes over time, we obtained distinct seasonal patterns of CH₄ production and emission for these two representative lakes (Fig. 5g and 5h; Fig. S10). In the cold, deep oligotrophic lake (Fig. 5g and Fig. S10a), winter to early spring ice cover (December-April) blocks CH₄ emissions such that lake CH₄ emissions are limited to the period between May and November. CH_4 production is highest $(8.0 \times 10^{-4} \text{ g CH}_4 \text{ m}^{-2} \text{ d}^{-1})$ in August and lowest $(8.0 \times 10^{-5} \text{ g CH}_4 \text{ m}^{-2} \text{ d}^{-1})$ in April. Almost all the produced CH₄ escapes the sediment via diffusion as gas bubbles do not form due to low CH₄ production rates and high-water pressure. However, the benthic CH₄ flux is subsequently largely oxidized in the well oxygenated deep water column. As a result, total lake CH₄ emissions are low (0 to 2.4×10⁻⁴ g CH₄ m⁻² d⁻¹) with a slight peak in October. In the shallow eutrophic lake (Fig. 5h and Fig. S10b), the warmer climate prevents ice formation on the lake surface, leading to an emission season about twice as long as under colder climatic conditions. CH₄ production (0.02 to 0.35 g CH₄ m⁻² d⁻¹) is >1000 times higher than that in cold, deep oligotrophic lake due to the higher nutrient loads, lower O₂ levels, higher irradiance as well as higher temperature (Fig. 5b). Higher CH₄ production rates, together with lower water pressure, drive the formation of gas bubbles, leading to a higher fraction of CH₄ emissions via the ebullitive pathway. The weaker stratification and the shorter transport time scale in the shallow lake limits CH₄ oxidation during diffusive transport, leading to ~900 times higher total CH₄ emissions compared to the deep, oligotrophic lake. Total lake CH₄ emissions are highest (0.21 g CH₄ m⁻² d⁻¹) in September and lowest (0.02 g CH₄ m⁻² d⁻¹) in February. By decomposing the collective responses of shallow and deep lakes into individual effects induced by trophic level, climate and lake depth using additional theoretical numerical simulations, we found that the trophic level exerts the most important control on CH4 dynamics, followed by climate, and finally, lake depth (Fig. S11-S14). Specifically, the yearly mean CH₄ production is





increased by a factor of 30 (from 0.003 to 0.089 g CH₄ m⁻² d⁻¹), and the yearly mean CH₄ emission is increased by a factor of 44 (from 0.0013 to 0.057 g CH₄ m⁻² d⁻¹) from oligotrophic to trophic status (i.e., [TDP] increased by 10 times) (Fig. S12). From cold to warm climate, the yearly mean CH₄ production and emission increase by a factor of 6 (0.0094 to 0.059 g CH₄ m⁻² d⁻¹) (Fig. S13), and a factor of 5 (0.0057 to 0.03 g CH₄ m⁻² d⁻¹), respectively. By increasing lake depth from 15 m to 35 m (Fig. S14), the CH₄ production rates remain almost the same, i.e., 0.02 g CH₄ m⁻² d⁻¹ for the yearly mean and 0.06 g CH₄ m⁻² d⁻¹ for the peak, while the CH₄ emissions are overall lower for the deeper lake.

$\textbf{3.2 Evaluation of simulated temporal lake } CH_{4} \ emissions \ against \ observations \ from \ four \ well-$

surveyed lakes

In Klöntal and Erssjön Lakes (Table 2, Fig. 6a and 6b), FLaMe captures the observed seasonal cycles of CH₄ emissions well, albeit with almost a one-month delay. As a result, the simulated CH₄ fluxes are slightly lower in the first half of the year and slightly higher in the second half. This lag between observations and model results is likely due to the use of idealized climate forcings but could also be attributed to the unresolved changes in water levels and in-lake TDP dynamics. In the Klöntal Lake (Fig. 6a), the observed CH₄ fluxes are exceptionally high in April (1.64 g CH₄ m⁻² d⁻¹) and July (5.03 g CH₄ m⁻² d⁻¹), interrupting the normal seasonal cycles. These abrupt observed emissions might reflect the contributions from storage fluxes that are not well captured by FLaMe. Apart from these two months with exceptionally high fluxes, the observational data indicates peak emissions of 3.18 g CH₄ m⁻² d⁻¹ in August and no emissions during the ice-covered period. FLaMe simulates similar fluxes, with a peak of 3.4 g CH₄ m⁻² d⁻¹ in September (and 3.17 g CH₄ m⁻² d⁻¹ in August), and a null flux in January–February when the model predicts ice formation. In the Erssjön Lake (Fig. 6b),





712 emissions during the ice-covered period, whereas FLaMe simulates a peak emission of 18.76 g CH₄ m⁻² d⁻¹ in August (and 12.82 g CH₄ m⁻² d⁻¹ in July), and no flux in February. Moreover, the simulated 713 714 CH₄ fluxes are exceptionally high in April (11.10 g CH₄ m⁻² d⁻¹) due to the release of a storage fluxes 715 that does not seem to be recorded by the observations. These high CH4 fluxes attributed to storage 716 and lake turnover are usually associated with large variability, i.e., in Klöntal Lake (Fig. 6a), the 717 observed variability (standard deviation, SD) in CH₄ flux in July is almost 8-fold larger than the 718 simulated one, whereas in Erssjön Lake (Fig. 6b), the simulated SD in CH₄ flux in April is almost 6-719 fold larger than that of the observed one. This suggests that both in-situ measurements and FLaMe 720 struggle to accurately capture the storage fluxes. Apart from these storage fluxes, we found that the 721 SDs of CH₄ fluxes simulated by FLaMe are lower than those observed for most months, indicating a 722 more stable behavior in the simulations compared to the observations across the multi-year period 723 considered here. 724 For the Upper Mystic and Villasjön Lakes (Fig. 6c and 6d), the observed temporal patterns of 725 CH₄ fluxes appear more erratic, either due to the dominant role of short-term water level fluctuations 726 or due to the complex ice cover dynamics. For the Upper Mystic Lake (Fig. 6c), the observed CH₄ 727 fluxes are irregular or fluctuating (0–17.6 g CH₄ m⁻² d⁻¹) over the year, a pattern which was explained 728 by dynamic variations of lake water levels (Varadharajan, 2009). Since in-situ water level 729 measurements are lacking, the simulated temporal variations cannot capture these observed erratic 730 patterns well. Our model produces a smoother seasonal cycle of monthly-mean CH₄ fluxes over the year, i.e., high fluxes (10.02–13.38 g CH₄ m⁻² d⁻¹) during the productive season (August–October), 731 732 and low fluxes (0.02-7.56 g CH₄ m⁻² d⁻¹) during the other months. Moreover, the model predicts a

observational data report a peak in CH₄ emission reaching 13.48 g CH₄ m⁻² d⁻¹ in July and no





734

735

736

737

738

739

740

741

742

743

744

745

746

747

748

749

750

751

752

753

754

weak storage flux occurring in November (10.20 g CH₄ m⁻² d⁻¹). For the Villasjön Lake (Fig. 6d), the observed CH₄ fluxes are limited to the period of June–October, due to the long ice cover period induced by the cold climate. FLaMe captures the observed ice-cover period well and produces similar seasonal cycles of CH₄ fluxes. The simulated means and SDs are very close to observations in June and July, but both, means and SDs, are much lower than observations in August, September, and October.

In summary, despite the use of idealized climatic forcing and neglecting variations in lake area and water level, FLaMe broadly captures the observed temporal patterns of monthly mean emissions, albeit sometimes with small delays or diverging extents of high emissions periods. The SDs of simulated CH₄ fluxes are also usually lower than the observed values, which is to be expected considering that our model is not designed to capture high-frequency fluctuations of CH4 fluxes. The largest biases can be found in the estimations of storage fluxes (timing and magnitude), probably due to 1) the difficulty of capturing these fluxes with existing measurement instruments and techniques, 2) the possibility of methane oxidation with greater than expected values during turnover and ice-out (Mayr et al., 2020; Zimmermann et al., 2019; Pajala et al., 2022) and 3) the lack of in-situ measurements of climate conditions, dynamical water levels, and dynamic TDP concentrations (Denfeld et al., 2018). Resolving these issues will require to assemble a much larger dataset of observed long time-series of CH₄ fluxes and associated physical and biogeochemical variables. To help further calibrate and evaluate the model, this much larger pool of observations should span a broader range of environmental conditions to be more representative of the lake CH₄ dynamics on the continental to global scales. Overall, given the scarce spatiotemporal observations and the limited possibility to validate current knowledge on process regulation in fields, it is difficult for all existing





models to produce the details of the CH₄ dynamics in specific single lakes. Hence, the temporal patterns of CH₄ fluxes simulated by FLaMe v1.0 are seen as acceptable, as its main focus is to capture the broad spatio-temporal patterns of CH₄ emissions across the thousands of lakes that need to be accounted for in large-scale applications (see section 3.3).

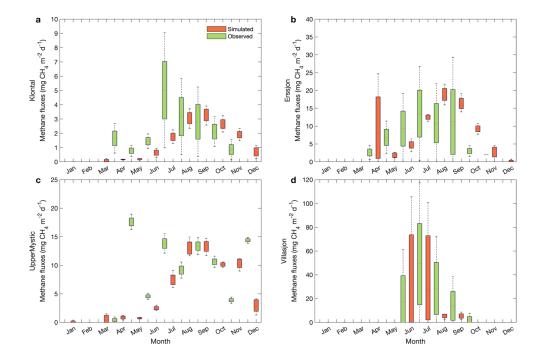


Fig. 6. Evaluation of FLaMe against monthly mean CH₄ fluxes recorded in long time-series of observations in four real lakes. (a) Klöntal, (b) Erssjön, (c) Upper Mystic, and (d) Villasjön. The detailed lake characteristics are listed in Table 2. The climate forcings for these four lakes are extracted from GSWP3-W5E5 model from ISIMIP3a. Note the different scales of CH₄ emissions in each lake.



766

767

768

769

770

771

772

773

774

775

776

777

778

779

780

781

782

783



3.3 FLaMe application on the European domain

3.3.1 Evaluation of FLaMe in European lakes

In the European scale application of FLaMe, we first evaluated the simulated F_{PP} against the empirical ranges reported by Wetzell (2001) for lakes under ultraoligotrophic (0-5 µgP L-1), oligotrophic (5–10 μgP L⁻¹), mesotrophic (10–30 μgP L⁻¹), and eutrophic (>30 μgP L⁻¹) conditions (Fig. 7 and Fig. S18). Figure 7 shows that, under different trophic status, the means and medians of F_{PP} simulated by FLaMe (for 953 representative lakes) fall well within the reported ranges. Slight deviations could only be observed in ultraoligotrophic lake for which the model tends to slightly overestimate F_{PP} (Fig. 7a). Ultraoligotrophic and oligotrophic lakes reveal very similar mean and median of F_{PP} that fall at the higher ends of the ranges specified by Wetzel (2001) or even exceed it in the case of ultraoligotrophic lakes. In turn, mesotrophic and eutrophic lakes reveal mean and median F_{PP} that fall at the lower ends of the ranges specified by Wetzel (2001). This slight difference of simulated versus observed F_{PP} in lakes with different trophic conditions can be explained by the relatively low value of $K_{s,P}$ (90 µg L⁻¹) compared to the concentration of [TDP] (Fig. S7–S8), as well as the simplified representation of lake primary production in our model. When extending the representative lakes to all real lakes in the European domain (n=108407), the median and mean of simulated F_{PP} are still within the specified ranges but are reduced slightly for all trophic status (Fig. S18), attributed to the positively skewed distribution of [TDP] (Fig. S8), i.e., many lakes have a low [TDP].



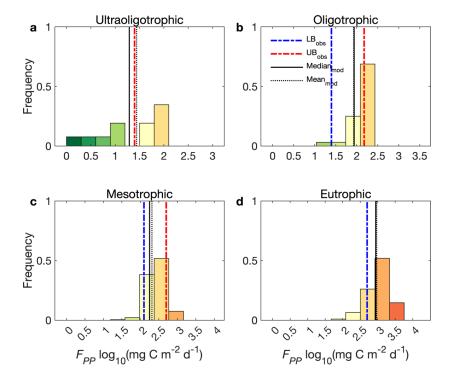


Fig. 7. Comparison of simulated primary production (F_{PP}) with empirical estimates reported by Wetzel (2001). The histograms show the frequency distributions of simulated F_{PP} (log scale) for 953 representative lakes that are grouped into ultraoligotrophic (0–5 μ gP L⁻¹), oligotrophic (5–10 μ gP L⁻¹), mesotrophic (10–30 μ gP L⁻¹), and eutrophic (>30 μ gP L⁻¹) lakes. In the figure, blue and red dashed lines are the lower and upper bounds (LB_{obs} and UB_{obs}), respectively, of empirical ranges reported by Wetzel (2001) in this class of lakes; Black solid and dotted lines are the median_{mod} and mean_{mod}, respectively, of simulated F_{PP} for this class of lakes.

Next, we evaluated the simulated diffusive and ebullitive CH₄ emission rates against measurements in boreal and central European regions during late summer (August–September, 2010–2011) synthesized by Rinta *et al.* (2017) (Fig. 8 and Fig. S19). As Rinta *et al.* (2017) compiled *in-situ*



796

797

798

799

800

801

802

803

804

805

806

807

808

809

810

811

812

813

814

815

816

817



measurements of diffusive and ebullitive CH₄ emission rates from 17 boreal lakes (in southern Finland and Sweden) and 30 lakes of central European lakes (in The Netherlands, Germany and Switzerland), we extracted the mean CH₄ emission rates during August-September for representative lakes located in the grid cells corresponding to these two regions. Results indicate that the simulated diffusive CH₄ emissions for boreal European lakes (Fig. 8) agree well with the observations; yet the simulated ebullitive CH4 emissions are slightly higher than the observations, leading to slightly higher total emissions. For central European lakes, the simulated diffusive CH₄ emissions are slightly lower than the observations, while the simulated ebullitive CH₄ emissions are slightly higher, leading to a good agreement in the total emissions (Fig. 8). Moreover, Rinta et al. (2017) reported 6 and 27 times higher diffusive and ebullitive fluxes in central Europe, respectively, while our model simulates a smaller contrast of a 3- and 7-fold difference. This smaller contrast in the simulation can likely be explained by the higher variability in measurements, reflecting diverse climate, light and catchment properties in real lakes, while the variabilities in the simulated fluxes are significantly lower, probably due to more homogeneous representations of environmental conditions in the FLaMe simulations. Specifically, the large differences in measured CH₄ emissions in boreal and central European lakes are attributed to their distinct characteristics, including climate (colder and dryer in the boreal region), light regime (larger absorbance in the boreal region) and catchment properties, in particular land-use (dominance of forests and smaller fraction of managed agricultural land in the boreal region). However, in FLaMe, the catchment properties are not fully captured by our sole, simplified indicator of [TDP], such that the differences between boreal and central European lakes are underestimated. The coarse resolution of our model also likely reduces the represented range of climate conditions in our simulations compared to those experienced by the sampled lakes. In the meantime, observations





are also associated with uncertainties, because measurements were not continuous in time and might
thus not be fully representative of the late summer-early fall period, as well as sampling and
measuring CH₄ emissions, in particular via the ebullitive pathway, is all but a trivial task.
Nevertheless, the above evaluation of FLaMe against observations overall reveals the ability of our
model to reproduce broadly observed patterns in primary production and CH₄ emissions observed
across distinct trophic status and landscapes.



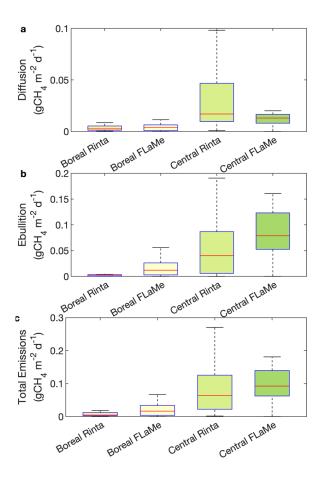


Fig. 8. Comparison of simulated diffusive (top), ebullitive (middle) and total (bottom) CH₄ emission rates with the measurements complied by Rinta *et al.* (2017). The datasets reported by Rinta *et al.* (2017) comprises the diffusive, ebullitive and total emission rates from 17 boreal lakes in Finland and Sweden and 30 lakes of central European lakes in The Netherlands, Germany and Switzerland. The boxes represent the 25% and 75% quartiles, and the whiskers cover the 95% confidence intervals. The same figure with a log scale is presented in Fig. S19.



832

833

834

835

836

837

838

839

840

841

842

843

844

845

846

847

848

849

850

851

852



3.3.2 European scale assessment of lake CH₄ emissions

The continental-scale assessment indicates that European lakes smaller than 1000 km² have an annual mean emission of 0.97 Tg CH₄ yr⁻¹ from autochthonous phytoplankton production during the period of 2010–2016, of which 30% and 70% are through diffusive and ebullitive transport pathways, respectively (Fig. 9 and Fig. S20). The mean CH₄ emission rates per unit lake area amounts to 7.39 g CH₄ m⁻² yr⁻¹, while the mean CH₄ emission rates per unit land surface area amounts to 0.054 g CH₄ m⁻² yr⁻¹. Both emission rates decrease from South to North, despite the larger number of lakes and lake surface area in Northern Europe (Messager et al., 2016; Fig. S4). This south to north decrease can be explained by a much higher CH₄ emission rate in the South of Europe (reaching 109.6 g CH₄ m⁻² yr⁻¹) driven by much higher eutrophic status of southern lakes (together with higher temperatures), which outcompetes the effect of the larger lake area in the Scandinavian region and Finland (which contribute to ~30% of the European lake area). This latitudinal pattern of CH₄ emissions per unit lake area is broadly consistent with that reported by Johnson et al. (2022) based on observations. In terms of seasonal variability, our model results are in full agreement with the sparse data set of seasonally resolved observations (Tan et al., 2015) and show that European lakes as a whole act as a continuous CH₄ source including during the winter months. Moreover, the simulated CH₄ production and emission reveal a sharp 10-fold increase from late Spring to late Summer that is largely driven by the increase in ambient temperature and F_{PP} rates. These findings underscore the importance of accounting for seasonal variations in CH4 emissions when refining regional methane budgets (Tan et al., 2015; Guo et al., 2020; Johnson et al., 2022; Stavert et al., 2022). A simple extrapolation of observed summer emissions to the yearly timescale would thus lead to an overestimation of yearly mean fluxes. In addition, model results also reveal a slight time-lag between





the most favorable climate conditions (air temperature and light) and the maximum CH₄ production. This time lag in the model can be explained by the cascade of biogeochemical reactions (primary production, mineralization, O₂ depletion and onset of CH₄ production) that ultimately control benthic CH₄ fluxes, and the timescale of heat transfer from the lake surface to the deepest portion of our valley-shape lake bottom. This slight time-lag is further amplified by the time required for the benthic CH₄ to reach the water-air interface, although this effect is secondary due to the dominance of shallow lakes (with mean depth <10 m for 98.7% of lakes) within the European domain. Finally, the broad seasonal pattern in CH₄ emissions is complicated by the episodic releases of storage fluxes during lake turnovers which occur during spring (March and April; emissions>production) and fall (October and November; emission circa 85% of the production). Lake turnovers amplify total emissions for the duration of these short-lived events.

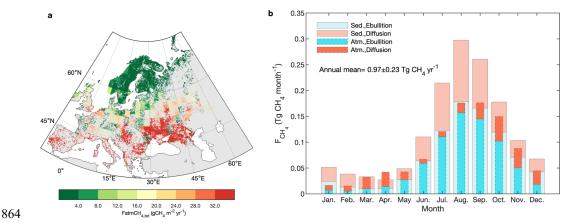


Fig. 9. Methane (CH₄) emissions from European lakes. (a) Spatial distribution of annual mean total CH₄ emissions (sum of diffusion and ebullition) for the period of 2010-2016, expressed in per unit of lake area. (b) Seasonality of total CH₄ production (dashed colors) and emission (full colors) fluxes and their split between ebullitive and diffusive pathways (period 2010-2016).



870

871

872

873

874

875

876

877

878

879

880

881

882

883

884

885

886

887

888

889

890



3.3.3 Sensitivity and uncertainty analysis

The sensitivity analysis of annual mean CH₄ emissions from European lakes to key model parameters (listed in Table 3) are summarized in Table 4. Table 4 indicates that the fraction of benthic organic matter mineralization channeled to methanogenesis (fmm) is the most sensitive parameter, and the increase (decrease) of f_{mm} by one SD leads to an increase (decrease) of European lake CH₄ emissions by 0.92 Tg CH₄ yr⁻¹ or 95% (0.67 Tg CH₄ yr⁻¹ or 69%). This is intuitive as a higher fraction of carbon channeled to methanogenesis will increase the continental scale CH₄ emissions, although the response is nonlinear. The second and third most sensitive parameters are the maximum carbon fixation rate per unit of Chlorophyll-a $(P_{chl,max})$ and the half saturation constant of phosphorus $(K_{s,P})$. An increase (decrease) of $P_{chl,max}$ by one SD could increase (decrease) the European lake CH₄ emissions by 0.77 Tg CH₄ yr⁻¹ or 79% (0.63 Tg CH₄ yr⁻¹ or 65%). This is again logical as a higher $P_{chl,max}$ indicates a stronger capacity of phytoplankton to assimilate carbon, thus resulting in higher amounts of organic carbon available for CH₄ production and emissions. The increase (decrease) of $K_{s,P}$ by one SD decreases (increases) the European lake CH₄ emissions by 0.46 Tg CH₄ yr⁻¹ or 48% (0.22 Tg CH₄ yr⁻¹ or 22%), a result which can be explained by a stronger TDP limitation of primary production when $K_{s,P}$ increases, resulting in lower CH₄ production and emissions. The next most sensitive parameters are the mineralization and burial rates (k20 and kbur), for which an increase (decrease) in k_{20} by one SD result in an increase (decrease) of European lake CH₄ emissions by 0.19 Tg CH₄ yr⁻¹ or 20% (0.39 Tg CH₄ yr⁻¹ or 40%), while an increase (decrease) of k_{bur} by one SD leads to a decrease (increase) of European lake CH₄ emissions by 0.35 Tg CH₄ yr ⁻¹ or 36% (0.21 Tg CH₄ yr⁻¹ or 22%). This is straightforward to interpret as a higher mineralization rate (k_{20}) will channel more mineralization into methanogenesis (and also via lower O2 levels in the lake), while a higher





892

893

894

895

896

897

898

899

900

901

902

903

904

905

906

907

908

909

910

911

burial rate (k_{bur}) translates to a lower relative amount of organic matter degradation, and thus lower CH₄ production and emissions.

The other parameters (including the shape parameter of the CH₄ production rate versus sediment depth α_{min} , the temperature dependence of mineralization θ , as well as the maximum CH₄ oxidation rate k_{max} and its temperature dependence $Q_{10,ox}$) are less sensitive, with their relative effects on European lake CH₄ emissions ranging from 1–20%. The shape parameter α_{min} can affect the CH₄ emissions as it determines the split between diffusive and ebullitive pathways, i.e., a higher α_{min} favors a higher fraction of CH₄ emitted to water and atmosphere through the diffusive pathway, a pathway that is more prone to oxidation thus lowering total CH₄ emissions. We also find that a higher temperature dependence of mineralization (θ) results in a lower CH₄ emission. This can be explained by the reference temperature of 20°C in the expression of the θ function, higher than the mean water temperature in most lakes, leading to a faster drop in mineralization for a larger θ when temperature is lower than 20°C. The parameter k_{max} barely impacts the total CH₄ emissions, as this parameter mostly influences the thickness of the water layers where the profiles of oxygen and methane overlap and the oxidation occurs, while the volume-integrated rates remain essentially unaltered (Regnier et al., 2011; Thullner and Regnier, 2019). As for the temperature dependence of oxidation ($Q_{10,ox}$), the sensitivity is even weaker because changing the $Q_{10,ox}$ value has a lower impact on the oxidation rates than changing k_{max} .

With the samples produced by the above sensitivity analysis and complemented by samples from additional tests, we utilized a Random Forest (RF) model to assess the uncertainty of European lake CH_4 emissions (see details in section 2.5.4). The RF model has a R^2 of 0.73 and Root of Mean Square





912 Error (RMSE) of 0.24 Tg CH₄ yr⁻¹ for the train set (Fig. 10a) and a R² of 0.52 and RMSE of 0.30 Tg 913 CH₄ yr⁻¹ for the out-of-bag samples (Fig. 10b), suggesting that the it can capture well the relationship 914 between model parameters and European lake CH₄ emissions. Using these ensembles of CH₄ 915 emissions, the uncertainty (or SD) of European lake CH₄ emissions associated with the choice of 916 biogeochemical parameter values was estimated as 0.23 Tg CH₄ yr⁻¹. Therefore, during the period of 917 2010-2016, the European lakes have an annual mean emission of 0.97±0.23 Tg CH₄ yr⁻¹. 918 With the RF model, we can also identify the importance of key model parameters involved as 919 predictors (Fig. 10c). We noticed that the first four leading parameters are also the most sensitive 920 parameters as identified in Table 4, while the importance of other parameters are slightly different 921 from the sensitivity analysis. This slight difference can be attributed to the interactions of model 922 parameters that are overlooked in the sensitivity analysis. Overall, from the sensitivity and uncertainty 923 analysis, we find that the European lake CH₄ emissions are strongly controlled by the carbon 924 biogeochemical dynamics, which, however, was not fully accounted for in previous lake models.



926

927

928

929



Table 4 Sensitivity of European lake CH₄ emissions (Tg CH₄ yr⁻¹) to key model parameters

Parameter se	Mean±SD		Mean±0.5SD		
		-SD	+SD	-0.5SD	+0.5SD
Primary production	P_{chl_max}	0.344	1.743	0.642	1.376
	$K_{s,P}$	1.432	0.754	1.170	0.852
Mineralization and	k_{20}	0.578	1.164	0.758	1.141
burial rates	k_{bur}	1.317	0.761	1.107	0.856
	θ	1.028	0.928	0.989	0.968
	f_{mm}	0.302	1.888	0.605	1.437
Methane oxidation	K_{max}	1.057	0.930	1.009	0.953
	$Q_{10,ox}$	0.992	0.983	0.978	0.973
Base value of the shape parameter	$lpha_{min}$	1.222	0.840	1.077	0.891

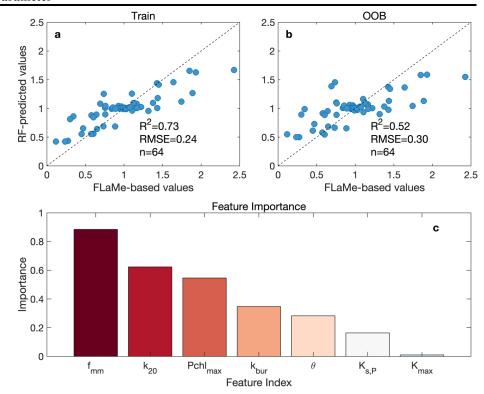


Fig. 10. Random Forest (RF) model for the uncertainty analysis. (a) and (b) are the train and test (Out-of-

Bag prediction) of the RF model. (c) shows the importance of key model parameters. Note that the





parameters of a_{min} and $Q_{10,ox}$ are excluded from illustration due to their second order of importance

(indicated by negative values).

4. Model limitations

We have illustrated that FLaMe is able to capture complex physical-biogeochemical behaviors for lakes with diverse settings and environmental controls. Specifically, the FLaMe model has been evaluated against (i) observational temporal variations of CH4 fluxes at four contrasting, well-surveyed real lakes, (ii) the empirical ranges of primary production under different trophic status reported by Wetzel (2001), and (iii) observational patterns of CH4 emissions against trophic and climate gradients spanning the European domain (Rinta *et al.*, 2017). Moreover, the European scale simulation produces a spatial pattern of lake CH4 emission rates consistent with observation-based upscaling approaches (Johnson *et al.*, 2022). This continental scale application also demonstrates the power of our modelling framework that rests on a lake clustering approach and on a routing of nutrient (TDP) inputs from surrounding catchments to lakes that allow to account for eutrophication effects. Our results thus suggest that the FLaMe modelling framework performs well in providing reliable spatio-temporal patterns of lake CH4 emissions at the large scale. However, the results also pinpoint to several key aspects to be improved in the model and highlight critical data gaps that must be addressed in the future.

First, the organic carbon module only accounts for autochthonous OC production as the substrate for methanogenesis, but ignores the contribution of allochthonous OC inputs leached from the surrounding catchments, rivers and streamflow. This is based on the distinct reactivity of autochthonous and allochthonous OC inputs, with the latter being more refractory to microbial





activities (mineralization and decomposition). As a result, FLaMe may provide conservative estimates of CH₄ productions and emissions. However, neglecting the allochthonous C inputs may at the same time minimize the feedback of OC on light penetration, leading to systematically biased estimates (section 2.2.2.1). Moreover, transient lake phosphorus dynamics and the co-limitations by nitrogen, albeit assumed to be less important, are neglected and might increase the uncertainty in the estimates of CH₄ production and emission. In addition, our primary production model does not resolve the short-term (e.g., (sub)daily) dynamics of algae growth induced by climate variability, rendering model-data comparison more difficult. In future model developments, these limitations could be addressed by (i) integrating or routing the lake water, carbon and nutrient fluxes along the global river network, which would allow to simultaneously solve the issue of time-invariant lake water levels in current global lake models (Golub *et al.*, 2022), including ours; (ii) refining the carbon module by incorporating more dynamic models for algal growth as well as P and N uptake and recycling processes within lakes.

Second, several model assumptions and implementations are based on empirical or theoretical knowledge, which may lead to biases in the estimation of CH₄ fluxes. For instance, the present version of FLaMe (i.e., v1.0) neglects the plant-mediated emission pathway (trough rooted plant) in the littoral zone due to the lack of observational data for model calibration. Moreover, in our model, the lake is assumed to follow a "valley" shape. Although this is an advancement from the "bucket" shape used in previous process-based lake models of CH₄ emissions (e.g., LAKE 2.0, ABLM, and bLake4Me), it remains a simplified assumption that captures important but not all features of a realistic lake geometry. Furthermore, several benthic CH₄ processes are highly parameterized. For instance, the split between aerobic and anaerobic decomposition of organic matter is represented by





a single parameter f_{mm} and is determined based on the data compilation from Bastviken (2022). This simplification leads to the same temperature dependence of CH₄ processes occurring in the sediment as that of pelagic and benthic mineralization. This is a shortcoming although it should be noted that the overall temperature dependence of CH₄ emissions, which results from the combined effects of OC production, mineralization, and subsequent CH₄ processes, was found to fall well within the observed ranges reported by Aben *et al.* (2017) (Fig. S21). The split of diffusive and ebullitive CH₄ fluxes is also currently captured by an empirically determined threshold depth ($z_{cb,min}$) based on limited observations by Langenegger *et al.* (2019). Moreover, the effects of heat transfer and CH₄ bubbles migration in the sediment are not resolved, which may lead to biased simulation of CH₄ fluxes especially for the timing. These are simplified representations related to the highly complex pathways of CH₄ production and emission, which needs to be improved by more mechanistic representations of the biogeochemical processes controlling carbon cycling, CH₄ production and transport via diffusion and bubble ascent.

Third, different modules of the FLaMe model could benefit from more comprehensive calibration and evaluation but those are limited by data availability. Although FLaMe has been evaluated against several timeseries of observed data collected in four well-surveyed lakes with contrasted dynamics, a full evaluation in the context of large-scale application would benefit from a significantly larger and representative set of observational data. Moreover, the *in-situ* climate conditions may vary greatly from the grid-level forcings, and the lake water dynamics may also affect the CH₄ fluxes significantly (e.g., Upper Mystic Lake; Varadharajan, 2009). Thus, a full comprehensive set of *in-situ* measurements of climate, water level, physical and biogeochemical variables would be highly valuable for the purpose of further model development, calibration and evaluation. At the European





scale, we partly circumvented these limitations by evaluating lake primary production against the broad ranges reported by Wetzel (2001), and the simulated diffusive and ebullitive CH₄ fluxes across the environmental (nutrient and climate) gradients compiled by Rinta *et al.* (2017). In this context, complementary time-series of vertically resolved organic carbon, CH₄ and O₂ concentrations, as well as high frequency measurements of CH₄ fluxes capturing short-lived emissions via the storage and ebullitive pathways and covering heterogeneity of CH₄ fluxes in large lakes (Denfeld *et al.*, 2018; Mayr *et al.*, 2020; Zimmermann *et al.*, 2019) would help further calibrate and evaluate the FLaMe model. These measurements should be performed using a sufficiently large set of representative lakes covering the full range of lake morphologies, landscape properties, and climate.

5. Conclusion and outlook

In this study, we developed and tested a new process-based biogeochemical modeling framework (FLaMe) to simulate lake CH₄ fluxes on the large-scale and, as a "proof of concept", applied the model to European lakes. The physical lake model builds on the Canadian Small Lake Model (CSLM) and is coupled to a set of novel biogeochemical modules describing lake organic matter, oxygen and methane dynamics. We then showcased the abilities and performance of FLaMe by: (1) analyzing the overall behaviors of the coupled C-O₂-CH₄ dynamics in two representative cases (a deep oligotrophic lake driven by cold climate in Northern Europe and a shallow eutrophic lake driven by warm climate in Southern Europe) as well as their decomposition, and (2) evaluating simulated temporal patterns of CH₄ fluxes against observations at four well-surveyed lakes with long-term timeseries. Simulation results were consistent with our common knowledge of lake CH₄ dynamics, suggesting that FLaMe can capture the patterns of CH₄ production and emissions across different lake types as well as their responses to the changes in environment conditions, despite the complexity of underlying





biogeochemical processes. Furthermore, by applying the model to boreal and central European lakes, we showed that FLaMe captures well the observed magnitudes of both diffusive and ebullitive CH₄ fluxes as well as the difference between boreal and central lakes. Finally, at the European scale, FLaMe estimates total CH₄ emissions from lakes smaller than 1000 km² (n=108407, total area = 1.33x10⁵ km²) as 0.97±0.23 Tg CH₄ yr⁻¹. In addition, the model resolves spatial patterns and seasonal variations of CH₄ emissions, providing a comprehensive view of their contribution to regional methane budgets.

Despite some limitations in its current model configuration, this first version of FLaMe is a significant step forward in biogeochemical simulations of lake CH4 dynamics. The model explicitly incorporates the dynamics of depth-integrated organic carbon cycling, such that the responses of organic carbon to climate and environmental change can be accounted for in estimating CH4 emissions. We also have incorporated the primary production as a function of total dissolved phosphorus loads from the surrounding catchments, allowing us to evaluate for the first time the impact of eutrophication on CH4 emissions in a quantitative way. Moreover, our model is of intermediate complexity, and is thus designed for large scale applications. Although the model was run here at a coarse spatial resolution, its parallelized version offers the possibility to carry simulations at a finer resolution in the future. With these advancements, our model can be used to resolve the spatio-temporal variability of CH4 emissions at regional and global scales under past and future climates, and has the potential to be coupled to Earth System Models to investigate the feedback between climate warming and global lake CH4 emissions.





1037 Data availability 1038 The methane emission data for the four well-surveyed real lakes (Klöntal, Erssjön, Upper Mystic, and 1039 Villasjön) were obtained from Tan et al. (2024). The in-situ measurements of diffusive and ebullitive 1040 CH₄ emission rates in boreal and central European regions during late summer (August-September 1041 2010–2011) were obtained from Rinta et al. (2017). The lake characteristic information within Europe 1042 were obtained HydroLAKES 2016): from the database (Messager al. 1043 https://www.hydrosheds.org/products/hydrolakes. The meteorological variables from GSWP3-1044 W5E5 reanalysis product were obtained from Inter-Sectoral Impact Model Intercomparison Project (ISIMIP3a): https://www.isimip.org/gettingstarted/input-data-bias-adjustment/. 1045 1046 1047 Code availability 1048 The source codes for FLaMe (Fluxes of Lake Methane) model version 1.0 are available at: 1049 https://github.com/myFeng818/FLaMe-model-v1.0.git. The preprocessing and postprocessing codes 1050 for the model can be obtained upon request. 1051 1052 Acknowledgements 1053 This study was supported by the Fonds National de la Recherche Scientifique of Belgium (F.R.S.-1054 FRNS PDR T.0191.23), by the project of CLIMATE-SPACE RECCAP2: Global Land Carbon Budget and its Attribution to regional drivers, as well as by the project of ESM2025-Earth System 1055 1056 Models for the Future (101003536). We acknowledge the climate modelling groups involved in 1057 ISIMIP3a for producing and making available their model outputs. Computational resources have





1058 been provided by the Consortium des Équipements de Calcul Intensif (CÉCI), funded by the Fonds 1059 de la Recherche Scientifique de Belgique (F.R.S.-FNRS) under Grant No. 2.5020.11 and by the 1060 Walloon Region. 1061 1062 **Author contributions** M.M., M.F. and P.R. designed the study. M.M. and M.F. co-developed and tested the FLaMe model. 1063 1064 D.B., S.A., R.L., A.J., G.G.L., M.D.M., and Z.T. provided plenty of valuable suggestions related to 1065 the model development. D.B. and S.A. also provided constructive suggestions on model evaluation 1066 against measurements and manuscript writing. M.D.M. helped us in setting up the CSLM at the 1067 beginning of developing FLaMe, Z.T. provided us the methane emission data from ISIMIP lake 1068 datasets, and W.T. helped us in collecting climate forcings from ISIMIP3a. M.M. and M.F. wrote the 1069 first version of the manuscript, and all coauthors helped in improving the manuscript. 1070 1071 **Competing interests** 1072 The authors declare no competing interests. 1073 1074 Additional information 1075 Correspondence and requests for materials should be addressed to M.F. (Maoyuan.feng@ulb.be) 1076





- 1077 References
- 1078 Aben, R.C.H., Barros, N., van Donk, E. et al.: Cross continental increase in methane ebullition under climate
- 1079 change. Nat. Commun., 8, 1682. https://doi.org/10.1038/s41467-017-01535-y, 2017.
- 1080 Arístegui, J., Agustí, S. and Duarte, C. M.: Respiration in the dark ocean, Geophys. Res. Lett., 30, 1041,
- 1081 https:///doi.org/10.1029/2002GL016227, 2003.
- 1082 Bastviken D., Tranvik L. J., Downing, J. A., Crill, P. M., Enrich-Prast, A.: Freshwater methane emissions offset the
- 1083 continental carbon sink, Science, 331(6013), 50. https://doi/org/10.1126/science.1196808, 2011.
- 1084 Bastviken, D. (2022). Methane. In T. Mehner & K. Tockner (Eds.), Encyclopedia of Inland Waters (Second Edition)
- 1085 (pp. 136-154). Oxford: Elsevier.
- 1086 Bastviken, D., Cole, J., Pace, M., and Tranvik, L.: Methane emissions from lakes: Dependence of lake
- 1087 characteristics, two regional assessments, and a global estimate, Global Biogeochem. Cycles, 18, GB4009,
- 1088 https://doi/org/10.1029/2004GB002238, 2004.
- 1089 Behrenfeld, M. J. and Falkowski P. G.: Photosynthetic rates derived from satellite-based chlorophyll
- 1090 concentration, Limnol. Oceanogr., 42, https://doi/org/10.4319/lo.1997.42.1.0001, 1997.
- 1091 Boehrer, B. and Schultze, M.: Stratification of lakes, Rev. Geophys., 46, 2006RG000210,
- 1092 https://doi.org/10.1029/2006RG000210, 2008.
- 1093 Bouwman, A. F., Beusen, A. H. W., Billen G.: Human alteration of the global nitrogen and phosphorus soil
- 1094 balances for the period 1970-2050, Global Biogeochem. Cycles, 23, GB0A04,
- 1095 https://doi/org/10.1029/2009GB003576, 2009.
- 1096 Canadell, J. G., Monteiro, P. M. S., Costa, M. H., et al.: Global carbon and other biogeochemical cycles and
- 1097 feedbacks, Climate Change 2021: The Physical Science Basis: Working Group I Contribution to the Sixth
- 1098 Assessment Report of the Intergovernmental Panel on Climate Change, Cambridge University
- 1099 Press, Cambridge, United Kingdom and New York, NY, USA, 673-816, 2021.
- 1100 Carlson, C. A., Ducklow, H. W., Michaels, A. F.: Annual flux of dissolved organic carbon from the euphotic zone
- in the northwestern Sargasso Sea, *Nature*, 397, 405–408, 1994
- 1102 Cole, J. J., and Caraco, N. F.: Atmospheric exchange of carbon dioxide in a low-wind oligotrophic lake measured
- 1103 by the addition of SF₆, Limnol. and Oceanogr., 4, https://doi/org/10.4319/lo.1998.43.4.0647, 1998.
- Deemer, B. R., Harrison, J. A., Li, S., et al.: Greenhouse Gas Emissions from Reservoir Water Surfaces: A New
- 1105 Global Synthesis. *Bioscience*, 66(11), 949-964. https://doi/org/10.1093/biosci/biw117, 2016.
- 1106 Deemer, B. R., & Holgerson, M. A.: Drivers of methane flux differ between lakes and reservoirs, complicating
- 1107 global upscaling efforts. J. Geophys. Res.-Biogeo., 126,
- $1108 \qquad \qquad e2019JG005600, \ https://doi.org/10.1029/2019JG005600, \ 2021.$
- 1109 DelSontro, T., Beaulieu, J.J., and Downing, J.A.: Greenhouse gas emissions from lakes and impoundments:





- Upscaling in the face of global change, *Limnol. Oceanogr. Lett.*, 3, 64-75, https://doi.org/10.1002/lol2.10073.
 2018
 Delwiche, K. and Hemond, H.F.: An enhanced bubble size sensor for long-term ebullition studies. *Limnol. Oceanogr. Methods*, 15, 821-835. https://doi.org/10.1002/lom3.10201, 2017
- Denfeld, B. A., Baulch, H. M., del Giorgio, P. A., Hampton, S. E., and Karlsson, J.: A synthesis of carbon dioxide and methane dynamics during the ice-covered period of northern lakes, *Limnol. Oceanogr. Lett.*, 3, 117-131. https://doi.org/10.1002/lo12.10079, 2018.
- Dlugokencky, E. J., Steele, L. P., Lang, P. M., Masarie, K. A.: The growth rate and distribution of atmospheric methane, *J. Geophys. Res.*, 99, 17021–17043, https://doi/org/10.1029/94JD01245, 1994.
- Frieler, K., *et al.*: Scenario setup and forcing data for impact model evaluation and impact attribution within the third round of the Inter-Sectoral Impact Model Intercomparison Project (ISIMIP3a), *Geosci. Model Dev.*, 17, 1–51, https://doi.org/10.5194/gmd-17-1-2024, 2024.
- Forster, P. M., *et al.*: Indicators of Global Climate Change 2023: annual update of key indicators of the state of the climate system and human influence, *Earth Syst. Sci. Data*, 16, 2625–2658, https://doi.org/10.5194/essd-16-2625-2024, 2024.
- Garnaud, C., MacKay, M., & Fortin, V.: A one-dimensional lake model in ECCC's land surface prediction system. *J. Adv. Model. Earth Syst.*, 14, e2021MS002861. https://doi.org/10.1029/2021MS002861, 2022.
- Gatley, D. P., Herrmann, S., & Kretzschmar, H. J.: A twenty-first century molar mass for dry air, *HVAC&R Research*, *14*(5), 655–662. https://doi.org/10.1080/10789669.2008.10391032, 2008.
- Golub, M., *et al.*: A framework for ensemble modelling of climate change impacts on lakes worldwide: the ISIMIP Lake Sector, Geosci. Model Dev., 15, 4597–4623, https://doi.org/10.5194/gmd-15-4597-2022, 2022.
- Guillemette, F., von Wachenfeldt, E., Kothawala, D. N., Bastviken, D., Tranvik, L. J.: Preferential sequestration of terrestrial organic matter in boreal lake sediments, *J. Geophys. Res. Biogeosci.*, 122, 863–874, https://doi.org/10.1002/2016JG003735, 2017.
- Hanson, P. C., Hamilton, D. P., Stanley, E. H., Preston, N., Langman, O. C., Kara, E. L.: Fate of Allochthonous
 Dissolved Organic Carbon in Lakes: A Quantitative Approach. *PLoS One*, 6(7): e21884,
 https://doi.org/10.1371/journal.pone.0021884, 2011.
- Hanson, P. C., Buffam, I., Rusak, J. A., Stanley, E. H., Watras, C.: Quantifying lake allochthonous organic carbon
 budgets using a simple equilibrium model, *Limnol. Oceanogr.*, 59, https://doi/org/10.4319/lo.2014.59.1.0167,
 2014
- Harrison, J. A., Prairie, Y. T., Mercier-Blais, S., Soued, C.: Year-2020 global distribution and pathways of reservoir methane and carbon dioxide emissions according to the greenhouse gas from reservoirs (G-res) model, *Global Biogeochem. Cycles*, 35, e2020GB006888. https://doi.org/10.1029/2020GB006888, 2021.





- 1143 Holgerson, M., and Raymond, P.: Large contribution to inland water CO2 and CH4 emissions from very small
- ponds. *Nature Geosci.*, 9, 222–226. https://doi.org/10.1038/ngeo2654, 2016.
- 1145 Imberger, J.: The diurnal mixed layer, Limnol. Oceanogr., 30, 737–770, https://doi.org/10.4319/lo.1985.30.4.0737,
- 1146 1985
- 1147 Imboden, D.M., and Wüest, A.: Mixing Mechanisms in Lakes. In: Lerman, A., Imboden, D.M., Gat, J.R. (eds)
- Physics and Chemistry of Lakes. Springer, Berlin, Heidelberg. https://doi.org/10.1007/978-3-642-85132-2 4,
- 1149 1995.
- Lan, X., Thoning, K.W., and Dlugokencky, E.J.: Trends in globally-averaged CH₄, N²O, and SF₆ determined from
- NOAA Global Monitoring Laboratory measurements. https://doi.org/10.15138/P8XG-AA10, 2024
- 1152 Langenegger, T., Vachon, D., Donis, D., McGinnis, D.F.: What the bubble knows: Lake methane dynamics revealed
- by sediment gas bubble composition. Limnol. Oceanogr., 64: 1526-1544. https://doi.org/10.1002/lno.11133.
- 1154 2019.
- 1155 Lauerwald, R., Regnier, P., Figueiredo, V., Enrich-Prast, A., Bastviken, D., Lehner, B.: Natural lakes are a minor
- 1156 global source of N₂O to the atmosphere. Global Biogeochem. Cycles, 33, 1564-
- 1157 1581. https://doi.org/10.1029/2019GB006261, 2019.
- 1158 Lauerwald, R., Allen, G. H., Deemer, B. R., Liu, S., Maavara, T., Raymond, P., et al.: Inland water greenhouse gas
- 1159 budgets for RECCAP2: 2. Regionalization and homogenization of estimates. Global Biogeochemical Cycles,
- 37, e2022GB007658, https://doi.org/10.1029/2022GB007658, 2023.
- Lewis, W. M.: Global primary production of lakes: 19th Baldi Memorial Lecture, *Inland Waters*, 1(1), 1–28.
- 1162 https://doi.org/10.5268/IW-1.1.384, 2011.
- Liikanen, A., Murtoniemi, T., Tanskanen, H., Väisänen, T., Martikainen, P. J.: Effects of temperature and oxygen
- 1164 availability on greenhouse gas and nutrient dynamics in sediment of a eutrophic mid-boreal
- lake, Biogeochemistry, 59, 269–286. https://doi.org/10.1023/A:1016015526712_2002
- 1166 Maavara, T., Lauerwald, R., Regnier, P., Van Cappellen, P.: Global perturbation of organic carbon cycling by river
- damming, *Nat. Commun.* **8**, 15347. https://doi.org/10.1038/ncomms15347<u>.</u>2017.
- 1168 Maavara, T., Lauerwald, R., Laruelle, G. G., Akbarzadeh, Z., Bouskill, N. J., Van Cappellen, P., Regnier,
- P. Nitrous oxide emissions from inland waters: Are IPCC estimates too high? Glob Change Biol., 25, 473–
- 1170 448. https://doi.org/10.1111/gcb.14504, 2019.
- 1171 MacIntyre, S., Bastviken, D., Arneborg, L., Crowe, A. T., Karlsson, J., Andersson, A., Gålfalk, M., Rutgersson, A.,
- 1172 Podgrajsek, E., Melack, J. M.: Turbulence in a small boreal lake: Consequences for air-water gas exchange,
- 1173 Limnol. Oceanogr., 66(3):827-854. https://doi.org/10.1002/lno.11645, 2020.
- 1174 MacKay, M. D., Verseghy, D. L., Fortin, V., and Rennie, M. D.: Wintertime simulations of a boreal lake with the
- 1175 Canadian Small Lake Model, J. Hydrometeorol., 18, 2143–2160, https://doi.org/10.1175/JHM-D-16-0268.1,





- 1176 2017.
- 1177 MacKay, M. D.: A process-oriented small lake scheme for coupled climate modeling applications, J.
- 1178 *Hydrometeorol.*, 13, 1911–1924, https://doi.org/10.1175/JHM-D-11-0116.1, 2012.
- 1179 McGinnis, D. F., Greinert, J., Artemov, Y., Beaubien, S. E., Wüest, A.: Fate of rising methane bubbles in stratified
- 1180 waters: How much methane reaches the atmosphere? J. Geophys. Res., 111, C09007,
- 1181 https://doi.org/10.1029/2005JC003183, 2006
- Mendonça, R., Müller, R.A., Clow, D., Verpoorter, C., Raymond, P., Tranvik, L. J., Sobek, S.: Organic carbon
- 1183 burial in global lakes and reservoirs, Nat. Commun., 8, 1694, https://doi.org/10.1038/s41467-017-01789-6,
- 1184 2017
- 1185 Messager, M., Lehner, B., Grill, G., Nedeva, I., Schmitt, O.: Estimating the volume and age of water stored in global
- lakes using a geo-statistical approach. Nat. Commun., 7, 13603, https://doi.org/10.1038/ncomms13603,
- 1187 2016.Martin, J. H., Knauer, G. A., Karl, D. M., Broenkow, W. W.: VERTEX: carbon cycling in the northeast
- 1188 Pacific, Deep. Sea. Res. A., 34, 2, 267-285, https://doi.org/10.1016/0198-0149(87)90086-0, 1987.
- Mayorga, E., Seitzinger, S. P., Harrison, J. A., Dumont, E. Beusen, A. H. W., Bouwman, A. F., Fekete, B. M.,
- 1190 Kroeze, C., Van Drecht, G.: Global Nutrient Export from WaterSheds 2 (NEWS 2): Model development and
- implementation, *Environ. Model. Softw.*, 25, 7, 837-853, https://doi.org/10.1016/j.envsoft.2010.01.007, 2010.
- 1192 Mayr, M. J., Zimmermann, M., Dey, J., et al.: Growth and rapid succession of methanotrophs effectively limit
- 1193 methane release during lake overturn. Commun. Biol., 3, 108. https://doi.org/10.1038/s42003-020-0838-z,
- 1194 2020.
- Jackson, R., Saunois, M., Bousquet, P., Canadell, J. G., Poulter, B., Stavert, A. R., Bergamaschi, P., Niwa, Y.,
- 1196 Segers, A., Tsuruta, A.: Increasing anthropogenic methane emissions arise equally from agricultural and fossil
- 1197 fuel sources, Environ. Res. Lett., 15, 071002, https://doi.org/10.1088/1748-9326/ab9ed2, 2020.
- 1198 Johnson, M. S., Matthews, E., Du, J., Genovese, V., Bastviken, D.: Methane emission from global lakes: New
- spatiotemporal data and observation-driven modeling of methane dynamics indicates lower emissions, J.
- 1200 Geophys. Res.-Biogeo., 127, e2022JG006793. https://doi.org/10.1029/2022JG006793, 2022.
- 1201 Pajala, G., Sawakuchi, H. O., Rudberg, D., et al.: The effects of water column dissolved oxygen concentrations on
- lake methane emissions—Results from a whole-lake oxygenation experiment. J. Geophys. Res.: Biogeo.,
- 1203 128(11), e2022JG007185. doi:10.1029/2022jg007185, 2023.
- 1204 Petrescu, A. M. R., Qiu, C., Ciais, P., et al.: The consolidated European synthesis of CH₄ and N₂O emissions for
- the European Union and United Kingdom: 1990-2017, Earth Syst. Sci. Data, 13, 2307-2362,
- 1206 https://doi.org/10.5194/essd-13-2307-2021, 2021.
- 1207 Petrescu, A. M. R., Qiu, C., McGrath, M. J., et al.: The consolidated European synthesis of CH₄ and N₂O emissions
- for the European Union and United Kingdom, 1990-2019, Earth Syst. Sci. Data, 15, 1197-1268,
- 1209 https://doi.org/10.5194/essd-15-1197-2023, 2023.





- 1210 Rinta, P., Bastviken, D. Schilder, J., van Hardenbroek, M., Stötter, T., Heiri, O.: Higher Late Summer Methane
- 1211 Emission from Central Than Northern European Lakes, J. Limnol., 76 (1),
- 1212 https://doi.org/10.4081/jlimnol.2016.1475, 2016.
- 1213 Regnier, P., Dale, A.W., Arndt, S., LaRowe, D.E., Mogollón, J., Van Cappellen, P.: Quantitative analysis of
- 1214 anaerobic oxidation of methane (AOM) in marine sediments: A modeling perspective, Earth-Sci. Rev., 106,
- 1215 1–2, 105-130, https://doi.org/10.1016/j.earscirev.2011.01.002, 2011.
- 1216 Reynolds, C. S.: The ecology of phytoplankton, Cambridge University Press, 2006
- 1217 Rosentreter, J. A., Borges, A. V., Deemer, B. R., et al.: Half of global methane emissions come from highly variable
- 1218 aquatic ecosystem sources, Nat. Geosci., 14(4), 225-230, https://doi.org/10.1038/s41561-021-00715-2, 2021.
- 1219 Ruardij, P. & Van Raaphorst, W.: Benthic nutrient regeneration in the ERSEM ecosystem model of the North Sea,
- 1220 Neth. J. Sea Res., 33, 3-4, 453-483, https://doi.org/10.1016/0077-7579(95)90057-8, 1995.
- 1221 Saunois, M., Bousquet, P., Poulter, B., et al.: The global methane budget 2000–2012, Earth Syst. Sci. Data, 8, 697–
- 1222 751, https://doi.org/10.5194/essd-8-697-2016, 2016.
- 1223 Saunois, M., Stavert, A. R., Poulter, B., et al.: The Global Methane Budget 2000–2017, Earth Syst. Sci. Data, 12,
- 1224 1561–1623, https://doi.org/10.5194/essd-12-1561-2020, 2020.
- 1225 Saunois, M., Martinez, A., Poulter, B., et al., Global Methane Budget 2000–2020, Earth Syst. Sci. Data Discuss.,
- 1226 https://doi.org/10.5194/essd-2024-115, in review, 2024.
- 1227 Stavert, A. R., Saunois, M., Canadell, J. G., et al.: Regional trends and drivers of the global methane
- 1228 budget, Glob. Change Biol., 28, 182–200. https://doi.org/10.1111/gcb.15901, 2021.
- 1229 Stepanenko, V., Mammarella, I., Ojala, A., Miettinen, H., Lykosov, V., and Vesala, T.: LAKE 2.0: a model for
- temperature, methane, carbon dioxide and oxygen dynamics in lakes, Geosci. Model Dev., 9, 1977–2006,
- 1231 https://doi.org/10.5194/gmd-9-1977-2016, 2016.
- 1232 Tan, Z., Zhuang, Q., and Anthony, K. W.: Modeling methane emissions from arctic lakes: Model development and
- site-level study, J. Adv. Model. Earth Syst., 7, 459–483, https://doi.org/10.1002/2014MS000344, 2015.
- 1234 Tan, Z., Yao, H., Melack, J., Grossart, H.-P., Jansen, J., Balathandayuthabani, S., et al. (). A lake biogeochemistry
- 1235 model for global methane emissions: Model development, site-level validation, and global applicability. J. Adv.
- 1236 *Model. Earth Syst.*, 16, e2024MS004275. https://doi.org/ 10.1029/2024MS004275, 2024.
- 1237 Thottathil, S. D., Reis, P. C. J., Prairie, Y. T.: Methane oxidation kinetics in northern freshwater
- 1238 lakes. Biogeochemistry, 143(1), 105–116. https://www.jstor.org/stable/48701400_2019.
- 1239 Thullner, M., Regnier, P.: Microbial controls on the biogeochemical dynamics in the subsurface. Rev. Mineral.
- 1240 Geochem., 85 (1): 265–302. https://doi.org/10.2138/rmg.2019.85.9, 2019.
- 1241 Van Drecht, G., Bouwman, A. F., Harrison, J., Knoop, J. M.: Global nitrogen and phosphate in urban wastewater





1242 1970 2050, Global Cycles, 23, GB0A03, for the period to Biogeochem. 1243 https://doi.org/10.1029/2009GB003458, 2009. 1244 Varadharajan, C.: Magnitude and spatio-temporal variability of methane emissions from a eutrophic freshwater lake, 1245 Thesis (Ph. D.)--Massachusetts Institute of Technology, Dept. of Civil and Environmental Engineering, 2009. 1246 Verseghy, D. L., and MacKay, M. D.: Offline Implementation and Evaluation of the Canadian Small Lake Model 1247 with the Canadian Land Surface Scheme over Western Canada. J. Hydrometeor., 18, 1563-1248 1582, https://doi.org/10.1175/JHM-D-16-0272.1, 2017. 1249 Wanninkhof, R., Asher, W. E., Ho, D. T., Sweeney, C., McGillis, W. R.: Advances in quantifying air-sea gas 1250 exchange and environmental forcing, Ann. Rev. Mar. Sci., 1, 213-44, https://doi.org/ 1251 10.1146/annurev.marine.010908.163742, 2009. 1252 Wetzel, R.G.: Limnology: Lake and River Ecosystems. Third Edition, Academic Press, San Diego, p389, 2001. 1253 William, R., Georgiy, K., Matti, L.: Basin-scale circulation and heat fluxes in ice-covered lakes, Limnol. 1254 Oceanogr., 59, https://doi.org/10.4319/lo.2014.59.2.0445, 2014. 1255 Zhuang, Q., Guo, M., Melack, J.M., Lan, X., Tan, Z., Oh, Y., Leung, L. R.: Current and future global lake methane 1256 process-based modeling analysis. J. Geophys. Res.-Biogeo., 128, 1257 e2022JG007137, https://doi.org/10.1029/2022JG007137.2023. 1258 Zimmermann, M., Mayr, M. J., Bouffard, D., Eugster, W., Steinsberger, T., Wehrli, B., Brand, A. Bürgmann, H.: Lake overturn as a key driver for methane oxidation, preprint, https://doi.org/10.1101/689182, 2019. 1259